

# NEURAL NETWORK ENHANCED POLYCONVEXIFICATION OF ISOTROPIC ENERGY DENSITIES IN COMPUTATIONAL MECHANICS

L. BALAZI\*, T. NEUMEIER\*, M. A. PETER†, D. PETERSEIM†

**ABSTRACT.** We present a neural network approach for fast evaluation of parameter-dependent polyconvex envelopes, which are crucial in computational mechanics. Our method uses a neural network architecture that inherently encodes polyconvexity in the main variable by combining a feature extraction layer that computes the minors function on the signed singular value characterisation of isotropic energy densities with a partially input convex neural network (PICNN). Polyconvex underestimation is weakly enforced by penalisation during training, as are the symmetries of the function. As a guiding example, we focus on a well-known isotropic damage problem, reformulated in terms of signed singular values, and apply a splitting approach to reduce the dimensionality of the parameter space, thereby making training more tractable. Numerical experiments show that the networks achieve sufficient accuracy for engineering applications while providing high compression and significant speed-up over traditional polyconvexification schemes. Most importantly, the network adapts to varying physical or material parameters, enabling real-time polyconvexification in large-scale computational mechanics scenarios.

**Key words.** Polyconvexity, input convex neural network, relaxation, isotropic damage model, parameter-dependent

**AMS subject classifications.** 49J45, 49J10, 74G65, 74B20, 68T07, 74A45

## 1. INTRODUCTION

Many relevant problems in solid mechanics seek to minimise the deformations  $u: \Omega \rightarrow \mathbb{R}^d$  of a body  $\Omega$  in spatial dimension  $d \in \{2, 3\}$  with respect to the energy functional

$$(1) \quad I(u) = \int_{\Omega} W(\nabla u; \zeta) \, dx,$$

where the energy density  $W: \mathbb{R}^{d \times d} \times \mathbb{R}^p \rightarrow \mathbb{R}_{\infty} := \mathbb{R} \cup \{\infty\}$  is defined over a suitable class of admissible functions. The vector  $\zeta \in \mathbb{R}^p$  represents spatially varying parameters, including material history, damage evolution or phase information. In many established engineering models, the density  $W$  is either inherently nonconvex or develops nonconvexity as its parameters evolve, as in damage or phase transition models. Such nonconvexity not only poses significant mathematical challenges, including the potential non-existence of minimisers, but also leads to serious problems in numerical simulation, such as mesh dependence and reduced robustness.

Relaxing  $W$  via (semi-)convexification identifies bounds of infimising sequences for the original nonconvex problem, yielding robust and mesh insensitive numerical results. As shown in [Bal76, Bal77, Bal02], polyconvexity is well suited for nonlinear elasticity. However, an analytical polyconvex envelope  $W^{\text{pc}}$  is often not available, so computational relaxation methods are required. Conventional approaches include optimisation-based and computational geometry methods, such as relaxation algorithms approximating the rank-one convex hull [Dol99, DW00, Bar04, BKN<sup>+</sup>24, KNP<sup>+</sup>24, KNM<sup>+</sup>22, CD18] or dedicated algorithms for polyconvex envelopes

\* INSTITUTE OF MATHEMATICS, UNIVERSITY OF AUGSBURG, UNIVERSITÄTSSTR. 12A, 86159 AUGSBURG, GERMANY

† INSTITUTE OF MATHEMATICS & CENTRE FOR ADVANCED ANALYTICS AND PREDICTIVE SCIENCES (CAAPS), UNIVERSITY OF AUGSBURG, UNIVERSITÄTSSTR. 12A, 86159 AUGSBURG, GERMANY

*E-mail address:* {loic.balazi, timo.neumeier, malte.peter, daniel.peterseim}@uni-a.de.

*Date:* April 10, 2025.

The authors gratefully acknowledge funding from the German Research Foundation (DFG) within the Priority Programme 2256 *Variational Methods for Predicting Complex Phenomena in Engineering Structures and Materials* (project number 441154176, reference IDs PE1464/7-2 and PE2143/5-2). Furthermore, we would like to thank the Bavarian State Ministry of Science and the Arts for funding the Augsburg AI Production Network as part of the High-Tech Agenda Plus.

[Bar05, EBG13, BEG15]. However, these methods are often subject to the curse of high-dimensionality, since they require the mesh-based discretisation of the  $(d \times d)$ -dimensional space of deformation gradients. Polyconvexification algorithms further increase the dimensionality because they perform the convexification in the minors space of the deformation gradient. For isotropic functions, this dimensionality can be reduced by characterising the polyconvexity via signed singular values, as in [WP23] (see [NPPW24] for a corresponding polyconvexification algorithm). However, despite their efficiency, these algorithms remain resource and time consuming, especially when  $d = 3$ . As a result, conventional relaxation algorithms are often impractical for engineering applications that require iterative computations and multi-query evaluations of the polyconvex hull for varying parameter values.

For example, frameworks such as the isotropic pseudo-time incremental damage model introduced in [BO12] involve a  $(d \times d + 1)$ -parameter dependent family of convexification problems, consisting of the deformation gradient and the internal variable from the previous time step that captures the material history (see Section 2). Such parameter dependence introduces additional dimensionality as the material parameter  $\zeta$  can vary at any material point in  $\Omega$ . This requires the polyconvex envelope to be computed from scratch for each parameter configuration, resulting in a  $(d \times d + p)$ -dimensional problem. Overall, the accurate approximation of polyconvex envelope for parameter-dependent energy densities is of great importance for the practical application of computational relaxation techniques.

To overcome the computational challenges of conventional relaxation schemes and make them practically feasible, we propose a neural network-based approach that compresses the parameter-dependent polyconvex envelope into the parameters of a small-scale artificial neural network that incorporates intrinsic properties of the polyconvexification problem into its architecture. Our method exploits a design that encodes polyconvexity by combining a feature extraction layer, which computes the minors function based on a signed singular value characterisation of isotropic functions, with Input Convex Neural Networks (ICNNs). In addition, symmetry properties and upper-bound relationships are systematically enforced during training through penalty terms in the loss functional, ensuring that the network satisfies the necessary physical and mathematical constraints. This tailored approach not only speeds up the approximation of the polyconvex envelope, but also increases the reliability of the approximations in practical engineering applications.

Recent advances in neural networks, particularly through the development of ICNNs [AXK17], have enabled architectures that enforce convexity in energy density functions, a key requirement for accurate material modelling. For example, [AAF22, AF23] use ANNs to learn constitutive laws from stress-strain data, while preserving fundamental principles of solid mechanics through ICNNs that ensure material stability. Similarly, [KFM<sup>+</sup>22] and [KOMFW22] propose machine learning based constitutive models for finite deformation and electro-mechanically coupled behaviour respectively, using ICNNs to enforce hyperelasticity, anisotropy and polyconvexity. In [LKK<sup>+</sup>23], a neural network-based hyperelastic constitutive model is introduced that inherently satisfies standard constitutive conditions using ICNNs, while [VRPB25] designs multi-scale heterogeneous structures with spatially varying microstructures by incorporating physical principles such as polyconvexity, objectivity and thermodynamic consistency. More recently, [GKWM25] introduced convex signed singular value neural networks (CSSV-NN) for isotropic hyperelastic energy formulations, enabling the prediction of polyconvex hulls. Unlike [GKWM25], which learns polyconvex hulls directly from the function, our approach aims to learn polyconvex envelopes, potentially parameter-dependent, from reference envelopes obtained either analytically or via established algorithms. Other work has also explored ANNs for modelling the behaviour of mechanically sound materials without using ICNNs [LK23, FJB<sup>+</sup>21, TSRT22, TCT22, CG22].

The remaining parts of this paper are structured as follows. In Section 2 we introduce a leading engineering application by presenting a parameter-dependent family of energy densities arising from an isotropic damage problem. In Section 3 we recall the signed singular value formulation of the polyconvex envelope for isotropic functions, while Section 4 introduces the properties preserving neural networks that enforce polyconvexity, symmetries and the upper bound relation. Finally, Sections 5 and 6 provides numerical examples including both mathematical

benchmarks and the engineering isotropic damage formulation (rewritten in the signed singular value framework and parameter-reduced via a splitting approach).

## 2. ISOTROPIC DAMAGE PROBLEM: A GUIDING EXAMPLE

As a guiding example for our accelerated convexification approach, we briefly recall the isotropic damage model introduced in [BO12] which is of importance in engineering applications and reflects a typical example of parameter-dependent polyconvexification of a family of functions. We begin by briefly recalling the necessary ingredients of continuum mechanical energy densities in the undamaged setting.

Let  $F$  denote the deformation gradient, i.e.  $F = \nabla u$  as introduced in (1). In this work, two different effective hyperelastic strain energy density functions  $\psi^0$  are considered: the Saint Venant–Kirchhoff model, representing the special case of a linear stress–strain relation in a Lagrangian formulation, and a compressible neo-Hookean model showing a nonlinear response. The Saint Venant–Kirchhoff model reads

$$(2) \quad \psi_{\text{STVK}}^0(F) = \frac{\mu}{4} \|F^T F - \mathbb{I}\|^2 + \frac{\lambda}{8} (\|F\|^2 - d)^2,$$

and the neo-Hookean model reads

$$(3) \quad \psi_{\text{NH}}^0(F) = \frac{\mu}{2} (\text{tr}(F^T F) - d) - \mu \ln(\det F) + \frac{\lambda}{2} \ln(\det F)^2,$$

where  $\lambda$  and  $\mu$  are the Lamé constants (and  $d$  is the spatial dimension).

We now turn to the formulation of the pseudo-time incremental energy density function capturing isotropic damage for the time step  $k \rightarrow k+1$ , which was derived in [BO12, Equation (20)], as

$$(4) \quad \begin{aligned} W(F_{k+1}; F_k, \alpha_k) &= \psi(F_{k+1}, p(F_{k+1}; \alpha_k)) - \psi(F_k, \alpha_k) \\ &+ p(F_{k+1}; \alpha_k) D(p(F_{k+1}; \alpha_k)) - \alpha_k D(\alpha_k) - \bar{D}(p(F_{k+1}; \alpha_k)) + \bar{D}(\alpha_k). \end{aligned}$$

In (4), the scalar parameter  $\alpha_k \in \mathbb{R}$  and the matrix  $F_k \in \mathbb{R}^{d \times d}$  denote the internal variable and deformation gradient, respectively, from the previous pseudo-time step  $k$  and are in this sense parameters for the step  $k+1$ , i.e. fixed and assumed to be known. The strain energy density function  $\psi$  is of the form

$$(5) \quad \psi(F, \alpha) = (1 - D(\alpha)) \psi^0(F),$$

and consists of the multiplication of the  $(1 - D)$  reduction factor and the virtually undamaged strain energy density  $\psi^0$ , which is assumed to be isotropic, e.g. a Saint Venant–Kirchhoff (2) or a neo-Hookean (3) energy density. Within this formulation, the function  $D: \mathbb{R} \rightarrow [0, 1)$  denotes the non-decreasing exponential damage function which was considered in [Mie95]. It maps the internal variable  $\alpha$  to the interval  $[0, 1)$ , where 0 reflects the undamaged state and 1 the fully damaged state, and is of the form

$$(6) \quad D(\alpha) = d_\infty \left( 1 - \exp\left(-\frac{\alpha}{d_0}\right) \right),$$

where the parameter  $d_\infty \in (0, 1)$  is referred to as the *asymptotic limit*, i.e. the maximum possible damage, and  $d_0 \in \mathbb{R}^+$  is referred to as the *damage saturation* parameter. The reciprocal value of the latter is related to how fast the asymptotic limit  $d_\infty$  is reached. The function

$$\bar{D}(\alpha) = d_\infty \left( \alpha + d_0 \exp\left(-\frac{\alpha}{d_0}\right) \right)$$

is the antiderivative of  $D$ . The evolution of the internal variable  $\alpha_{k+1}$ , and consequently the evolution of the damage modelled by  $D(\alpha_{k+1})$ , is determined by a *path function*  $p$ , as

$$(7) \quad \alpha_{k+1} = p(F_{k+1}; \alpha_k) = \begin{cases} \psi^0(F_{k+1}) & \text{if } \psi^0(F_{k+1}) > \alpha_k, \\ \alpha_k & \text{else.} \end{cases}$$

The function  $W$  from (4) is nonconvex due to the damage evolution process, i.e. the influence of the path function  $p$ . From a theoretical perspective, this nonconvexity raises the problem

that the existence of minimisers can not be guaranteed. From a numerical point of view, this lack of convexity poses several challenges including stability issues, non-convergence, and the development of oscillations in the simulation of boundary value problems, for this specific example see e.g. [BO12, BKN<sup>+</sup>24, KNP<sup>+</sup>24, KNM<sup>+</sup>22] where the relaxation was addressed by means of rank-one convexification.

### 3. POLYCONVEXIFICATION OF ISOTROPIC FUNCTIONS

We now turn to our polyconvexification approach and introduce a reformulation in terms of the signed singular values of the deformation gradient, which is the basis for our neural-network design. For ease of notation, we drop the parameter dependence and restrict to functions  $W: \mathbb{R}^{d \times d} \rightarrow \mathbb{R}_\infty$  in this Section. The parameter-dependent formulation is given in direct analogy by adding the parameter vector  $\zeta$  and considering the function  $W(\cdot; \zeta)$ .

Assume the function  $W$  to be isotropic, we leverage the characterisation of isotropic functions via their signed singular values to reduce dimensionality in the representation. The problem of polyconvexification of an isotropic function can be reduced to the convexification of a function acting on the manifold characterised by the minors of the signed singular values. This formulation is advantageous in the numerical treatment of the problem since it is formulated for the space of signed singular values in  $\mathbb{R}^d$ , instead of  $\mathbb{R}^{d \times d}$ , the domain of  $W$ , and hence reduces dimensionality in the representative grid, rendering it an efficient approach for computing the polyconvex envelope using conventional algorithms, see e.g. [NPPW24] and Section 6.3, or as in the scope of this work, for learning and predicting the polyconvex envelope via structure-preserving artificial neural networks.

Let  $d \in \{2, 3\}$  and let  $W: \mathbb{R}^{d \times d} \rightarrow \mathbb{R}_\infty$  be a function which maps  $(d \times d)$ -matrices to real scalars or infinity. We are interested in the polyconvex envelope, denoted  $W^{\text{pc}}$ , of the function  $W$ . The notion of polyconvexity relies on the minors of the matrices  $F \in \mathbb{R}^{d \times d}$ . Given the determinant  $\det(F)$  and the adjugate  $\text{adj}(F)$  of  $F$ , let

$$(8) \quad \mathcal{M}(F) = \begin{cases} (F, \det(F)) & \text{if } d = 2, \\ (F, \text{adj}(F), \det(F)) & \text{if } d = 3 \end{cases}$$

denote the minors of  $F$ , i.e.  $\mathcal{M}(F)$  is a vector of dimension  $K_d = 5$  if  $d = 2$  and  $K_d = 19$  if  $d = 3$ . A function  $V: \mathbb{R}^{d \times d} \rightarrow \mathbb{R}_\infty$  is said to be polyconvex if there exists a convex function  $G: \mathbb{R}^{K_d} \rightarrow \mathbb{R}_\infty$  such that for all  $F \in \mathbb{R}^{d \times d}$ ,

$$V(F) = G(\mathcal{M}(F)).$$

The polyconvex envelope  $W^{\text{pc}}(F): \mathbb{R}^{d \times d} \rightarrow \mathbb{R}_\infty$  of  $W$ , defined by the pointwise supremum

$$(9) \quad W^{\text{pc}}(F) = \sup\{V(F) \mid V: \mathbb{R}^{d \times d} \rightarrow \mathbb{R}_\infty \text{ polyconvex}, V \leq W\},$$

is the largest polyconvex function below  $W$ .

As we are interested in polyconvexity of isotropic functions, we make use of the results of [WP23]. We call  $W$  isotropic if and only if

$$W(F) = W(R_1 F R_2)$$

for all  $F \in \mathbb{R}^{d \times d}$  and all  $R_1, R_2 \in \mathcal{SO}(d)$  and we say that  $W$  is  $\mathcal{SO}(d) \times \mathcal{SO}(d)$ -invariant in this case, where  $\mathcal{SO}(d)$  denotes the special orthogonal group of  $(d \times d)$ -matrices. In particular, isotropic functions can be characterised by the signed singular values of their arguments.

Let  $0 \leq \sigma_1, \dots, \sigma_d \in \mathbb{R}$  denote the singular values of a matrix  $F \in \mathbb{R}^{d \times d}$ . Then  $\nu_1, \dots, \nu_d \in \mathbb{R}$  are called *signed singular values* of  $F$ , if they have the same absolute values as the singular values of  $F$ , i.e. up to permutation it holds  $|\nu_i| = \sigma_i$ , and their signs satisfy  $\text{sign}(\nu_1 \dots \nu_d) = \text{sign}(\det(F))$ . In this definition the signed singular values are only unique up to permutations in

$$\Pi_d = \left\{ P \text{diag}(\varepsilon) \in \mathcal{O}(d) \mid P \in \text{Perm}(d), \varepsilon \in \{-1, 1\}^d, \varepsilon_1 \dots \varepsilon_d = 1 \right\},$$

where  $\text{diag}$  refers to the diagonal matrix with entries given by the vector of its argument and  $\text{Perm}(d) \subset \{0, 1\}^{d \times d}$  denotes the set of permutation matrices. In what follows, we denote by  $\nu: \mathbb{R}^{d \times d} \rightarrow \mathbb{R}^d$  the signed singular value mapping assumed to be well-defined, e.g. by fixing the

order of the entries according to the magnitude of the absolute values and assuming positivity of the entries up on only one entry, i.e. assigning the sign of the determinant to a single fixed entry.

It is possible to identify the set of isotropic functions  $W: \mathbb{R}^{d \times d} \rightarrow \mathbb{R}_\infty$  with the set of  $\Pi_d$ -invariant functions  $\Phi: \mathbb{R}^d \rightarrow \mathbb{R}_\infty$ , i.e.  $\Phi(\hat{\nu}) = \Phi(S\hat{\nu})$  for all  $\hat{\nu} \in \mathbb{R}^d$  and all  $S \in \Pi_d$ . The identifications are given by

$$(10) \quad W(F) = \Phi(\nu(F)) \quad \text{and} \quad \Phi(\hat{\nu}) = W(\text{diag}(\hat{\nu}))$$

for all  $F \in \mathbb{R}^{d \times d}$  and for all vectors  $\hat{\nu} \in \mathbb{R}^d$ .

In analogy to the definition of polyconvexity based on the minors  $\mathcal{M}$  defined in (8), we introduce the notion of polyconvexity for the mapping  $\Phi$  by defining a lifting of the  $\hat{\nu}$  argument to a higher dimensional space. For  $d \in \{2, 3\}$ , we define  $k_d := 2^d - 1$  that is  $k_d = 3$  if  $d = 2$  and  $k_d = 7$  if  $d = 3$  and the mapping  $m: \mathbb{R}^d \rightarrow \mathbb{R}^{k_d}$  by

$$m(\hat{\nu}) = \begin{cases} (\hat{\nu}_1, \hat{\nu}_2, \hat{\nu}_1 \hat{\nu}_2) & \text{if } d = 2, \\ (\hat{\nu}_1, \hat{\nu}_2, \hat{\nu}_3, \hat{\nu}_2 \hat{\nu}_3, \hat{\nu}_3 \hat{\nu}_1, \hat{\nu}_1 \hat{\nu}_2, \hat{\nu}_1 \hat{\nu}_2 \hat{\nu}_3) & \text{if } d = 3. \end{cases}$$

We call  $m(\hat{\nu})$  the vector of minors of  $\hat{\nu} \in \mathbb{R}^d$ ; in the literature, this vector is also referred to as elementary polynomials. A  $\Pi_d$ -invariant function  $\Psi$  is called (signed singular value) polyconvex if there exists a convex function  $g: \mathbb{R}^{k_d} \rightarrow \mathbb{R}_\infty$  such that  $\Psi = g \circ m$ , see [WP23, Theorem 1]. The (signed singular value) polyconvex envelope of  $\Phi$  is defined in an analogous way to the  $(d \times d)$ -case by

$$(11) \quad \Phi^{\text{pc}}(\hat{\nu}) = \sup\{\Psi(\hat{\nu}) \mid \Psi: \mathbb{R}^d \rightarrow \mathbb{R}_\infty \text{ polyconvex}, \Psi \leq \Phi\}.$$

The same identifications as in (10) also hold for the polyconvex envelopes, [NPPW24, Remark 2.2], i.e.

$$(12) \quad W^{\text{pc}}(F) = \Phi^{\text{pc}}(\nu(F)) \quad \text{and} \quad \Phi^{\text{pc}}(\hat{\nu}) = W^{\text{pc}}(\text{diag}(\hat{\nu})).$$

Motivated by the identification (12), we restrict ourselves to the approximation of  $\Phi^{\text{pc}}$ . According to [NPPW24, Corollary 2.5], the polyconvex envelope  $\Phi^{\text{pc}}$  of  $\Phi$  can be obtained by

$$(13) \quad \Phi^{\text{pc}}(\hat{\nu}) = h^c(m(\hat{\nu})),$$

where  $h^c$  is the convex envelope of the function  $h$  acting in the lifted signed singular value space and defined by

$$h: \mathbb{R}^{k_d} \rightarrow \mathbb{R}_\infty, \quad x \mapsto \begin{cases} \Phi(\hat{\nu}) & \text{if } x = m(\hat{\nu}), \\ \infty & \text{else.} \end{cases}$$

The relation (13) transforms the polyconvexification problem of  $\Phi$  into a convexification problem of the function  $h$  in the lifted signed singular value space. Compared to the polyconvexification problem in the  $d \times d$  setting, this formulation reduces the dimensionality of the convexification manifold from  $d \times d$  to  $d$ , as shown in [NPPW24], thereby enabling an efficient numerical treatment.

#### 4. PROPERTIES-PRESERVING NEURAL NETWORKS

In what follows, we aim for the approximation of  $\Phi^{\text{pc}}: \mathbb{R}^d \times \mathbb{R}^p \rightarrow \mathbb{R}$  by a neural network denoted by  $\Phi_{\text{pred}}^{\text{pc}}: \mathbb{R}^d \times \mathbb{R}^p \rightarrow \mathbb{R}$ . This is done by approximating the convex envelope of the parameter dependent function  $h: \mathbb{R}^{k_d} \times \mathbb{R}^p \rightarrow \mathbb{R}_\infty$ , i.e.  $h^c$  from (13). Note that we restrict the function  $\Phi^{\text{pc}}$  and the output of the neural network  $\Phi_{\text{pred}}^{\text{pc}}$  to be finite valued. To simplify notation, in some formulas we denote the minors of the signed singular values as  $\hat{m} := m(\hat{\nu})$ .

**4.1. Neural Network: Theoretical Framework.** An artificial neural network [Cal20] is a mathematical model defined as a composition of functions, which are themselves defined as composition of other functions. This model can be conveniently represented as a network structure. In what follows, we present the basic notions regarding layers, weights, inputs and outputs of a general neural network.

We denote the layer number by the superscript  $\ell \in \{0, \dots, L\}$ , where  $\ell = 0$  denotes the input layer,  $\ell = 1$  the first hidden layer and  $\ell = L$  the output layer. The total number of hidden layers

is then equal to  $L - 1$ . The number of neurons in the  $\ell$ th layer is denoted by  $d^{(\ell)}$ . In particular,  $d^{(0)}$  denotes the number of inputs and  $d^{(L)}$  the number of outputs.

The system of weights is denoted by  $w_\ell^{(i,j)}$ , with  $1 \leq \ell \leq L$ ,  $0 \leq i \leq d^{(\ell-1)}$ ,  $1 \leq j \leq d^{(\ell)}$ . The weight  $w_\ell^{(i,j)}$  is associated with the edge joining the  $i$ th neuron in the layer  $\ell - 1$  to the  $j$ th neuron in the layer  $\ell$ . The weights  $w_\ell^{(0,j)} = b_\ell^{(j)}$  are regarded as biases. The total number of weights in a feedforward network is  $\sum_{\ell=1}^L d^{(\ell-1)}d^{(\ell)}$ .

The inputs to the network are denoted by  $z_0^{(j)}$ , with  $1 \leq j \leq d^{(0)}$ . We denote by  $z_\ell^{(j)}$  the output of the  $j$ th neuron in the layer  $\ell$  and  $z_L^{(j)}$  is the network output, with  $1 \leq \ell \leq d^{(L)}$ , and we write  $z_\ell^{(0)} = -1$ , the fake input linked to the bias. Consider the  $j$ th neuron in the layer  $\ell$ . First, the neuron collects the information from the previous layer as a weighted sum, leading the preactivation, and then applies an activation function  $g_\ell$  on this quantity, as

$$z_\ell^{(j)} = g_\ell \left( \sum_{i=1}^{d^{(\ell-1)}} w_\ell^{(i,j)} z_{\ell-1}^{(i)} - b_\ell^{(j)} \right),$$

or written compactly in the following matrix form

$$Z_\ell = g_\ell (W_\ell Z_{\ell-1} - B_\ell),$$

where

$$Z_\ell = (z_\ell^{(1)}, \dots, z_\ell^{(d^\ell)})^T, \quad W_\ell = (w_\ell^{(i,j)})_{i,j}, \quad B_\ell = (b_\ell^{(1)}, \dots, b_\ell^{(d^\ell)})^T.$$

Building on the characterisation of the (signed singular value) polyconvex envelope  $\Phi^{\text{PC}}$  in [Section 3](#), the goal is to construct a neural network approximation denoted by  $\Phi_{\text{pred}}^{\text{PC}}$  which rigorously preserves its physical properties. The architecture must ensure polyconvexity, meaning convexity with respect to the minors of the signed singular values. Additionally, it must satisfy the envelope inequality condition, enforcing the inequality  $\Phi^{\text{PC}} \leq \Phi$  as stated in [\(11\)](#). Finally, the network must respect the  $\Pi_d$ -invariance as symmetry property of the function  $\Phi$ . The following sections outline strategies to incorporate these characteristics of the function  $\Phi^{\text{PC}}$  into the design of the neural network.

**4.2. Enforcing the Polyconvexity.** In order to enforce the convexity in the minors  $m(\hat{\nu})$  of the input vector  $\hat{\nu}$ , a particular class of neural networks is employed: the so-called Input Convex Neural Networks (ICNN) introduced in [\[AXK17\]](#). In particular, in what follows, two variants of ICNN are presented: the fully input convex neural networks (FICNN) and the partially input convex neural networks (PICNN). Note that the illustrations already reflect the convexity with respect to the minors  $\hat{m}$ , i.e. the formulation to ensure polyconvexity. The change from the original input  $(\hat{\nu}, \zeta)$  of the function  $\Phi^{\text{PC}}$  to the input  $(m(\hat{\nu}), \zeta)$  of the function  $h^c$ , i.e. the transitioning from the signed singular values to the minors lifted signed singular values, can be interpreted as a hard-coded feature extracting layer in the overall network architecture.

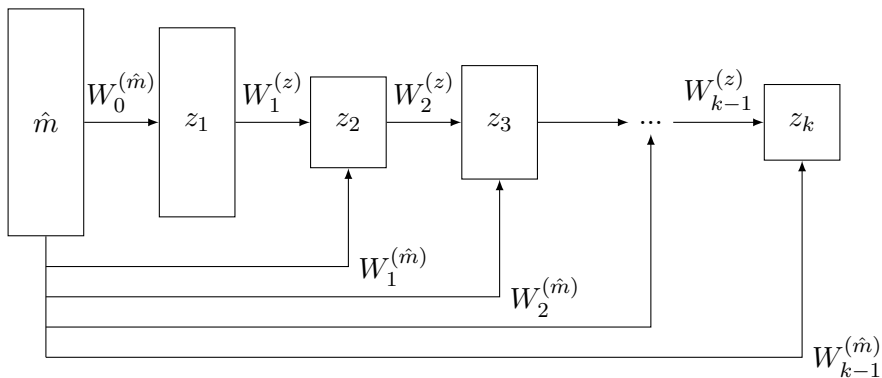


FIGURE 1. A fully input convex neural network (FICNN).

4.2.1. *Fully input convex neural networks (FICNN)*. The model illustrated in Figure 1 defines a neural network over the input  $\hat{m}$  using the recurrence for  $i = 0, \dots, k-1$ ,

$$z_{i+1} = g_i(W_i^{(z)} z_i + W_i^{(\hat{m})} \hat{m} + b_i),$$

where  $z_i$  denotes the layer activations (with  $z_0 = 0$ ,  $W_0^{(z)} \equiv 0$ ) and  $g_i$  are nonlinear activation functions. The overall network evaluation reads

$$\Phi_{\text{pred}}^{\text{pc}}(\hat{v}) := h_{\text{pred}}^c(\hat{m}; \theta) = z_k,$$

where  $h_{\text{pred}}^c$  is the neural network approximation of the function  $h^c$  defined in (13) and depends on  $\theta = \{W_{0:k-1}^{(\hat{m})}, W_{1:k-1}^{(z)}, b_{0:k-1}\}$ , the parameter vector collecting the weights and biases.

**Proposition 4.1.** *The function  $\Phi_{\text{pred}}^{\text{pc}}$  is polyconvex, that is  $h_{\text{pred}}^c(\cdot; \theta)$  is convex in  $\hat{m}$ , i.e. the minors  $m(\hat{v})$  of the signed singular values vector  $\hat{v}$ , provided that all  $W_{1:k-1}^{(z)}$  are non-negative and all activation functions  $g_i$  are convex and non-decreasing.*

The proof follows from the fact that non-negative sums of convex functions are also convex, and that the composition of a convex and nonconvex decreasing function is also convex. The constraint that the  $g_i$  are convex and non-decreasing is not particularly restrictive, since current nonlinear activation functions such as the ReLU or Softplus activation functions already satisfy this constraint. A review of convex activation functions is presented in [WWS23].

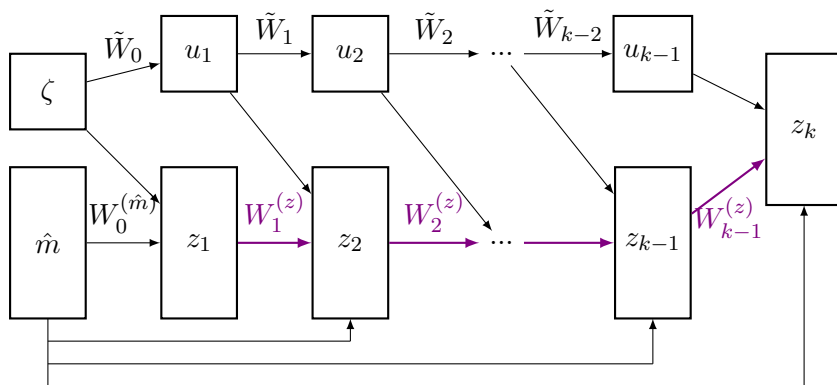


FIGURE 2. A partially input convex neural network (PICNN), coloured weights need to be non-negative to ensure convexity of the network in  $\hat{m}$ .

4.2.2. *Partially input convex neural networks (PICNN)*. The previous model, i.e. FICNN, provides convexity over the entire input of the neural network, which may in fact be a restriction on the allowable class of models. Furthermore, this full joint convexity is unnecessary in the setting where the convexity is required only over some inputs. This is why we present the partially input convex neural networks (PICNN), as introduced in [AXK17], which are convex over only some inputs of the network. The  $k$ -layer PICNN architecture (Figure 2) is defined by the recurrence for  $i = 0, \dots, k-1$ ,

$$u_{i+1} = \tilde{g}_i(\tilde{W}_i u_i + \tilde{b}_i),$$

$$z_{i+1} = g_i\left(W_i^{(z)}\left(z_i \circ \max([W_i^{(zu)} u_i + b_i^{(z)}], 0)\right) + W_i^{(\hat{m})}\left(\hat{m} \circ [W_i^{(\hat{m}u)} u_i + b_i^{(\hat{m})}]\right) + W_i^{(u)} u_i + b_i\right),$$

with  $u_0 = \zeta$ ,  $z_0 = 0$  and  $W_0^{(z)} = 0$  and

$$\Phi_{\text{pred}}^{\text{pc}}(\hat{v}; \zeta) := h_{\text{pred}}^c(\hat{m}; \zeta; \theta) = z_k$$

denotes the overall evaluation of the network. Moreover,  $h_{\text{pred}}^c$  is the neural network approximation of the function  $h^c$  defined in (13) and depends on  $\theta$ , the parameter vector collecting the weights and biases. The  $u_i \in \mathbb{R}^{n_i}$  and  $z_i \in \mathbb{R}^{m_i}$  denote the hidden units for the  $\zeta$ -path and  $\hat{m}$ -path,

and  $\circ$  denotes the Hadamard product, i.e. the element-wise product between two vectors. The functions  $g_i$  and  $\tilde{g}_i$  are activation functions.

**Proposition 4.2.** *The function  $\Phi_{\text{pred}}^{\text{DC}}(\cdot; \zeta)$  is polyconvex in the signed singular values vector  $\hat{\nu}$ , that is  $h_{\text{pred}}^{\text{C}}(\cdot; \zeta; \theta)$  is convex in  $\hat{m}$ , i.e. the minors  $m(\hat{\nu})$  of the signed singular values vector  $\hat{\nu}$ , provided that the weights  $W_{1:k-1}^{(z)}$  are non-negative, and all activation functions  $g_i$  associated with the  $\hat{m}$  path are convex and non-decreasing.*

In the present work, FICCN is employed when the function to be predicted does not depend on parameters but only on the signed singular values vector  $\hat{\nu}$ , and PICCN is employed when the function to be predicted depends on the signed singular values vector  $\hat{\nu}$  along with additional parameters  $\zeta$ . Indeed, the use of PICCN allows to ensure convexity with respect to the minors  $m(\hat{\nu})$  of the signed singular values vector  $\hat{\nu}$  while relaxing the constraints on the  $\zeta$ -path, allowing a better representation.

**Remark 4.3.** *Using ICNN is not the only way to enforce convexity (resp. polyconvexity). For instance, in [TSRT22] the convexity condition is ensured by penalisation with an additional term in the loss function that imposes positive-definiteness of the Hessian matrix. [TCT22] present a formulation based on neural ordinary differential equations (N-ODEs) in which polyconvexity of the strain energy is automatically satisfied by the proposed formulation. [CG22] considers enforcing convexity in the strong sense, by defining classes of surrogate models that satisfy the condition a priori. Their approach relies on simple integral representations to define an operator that transforms any arbitrary function (and in particular, a free neural network) into a convex function. [LK23] employ polyconvex activation functions and suitable network architectures to ensure polyconvexity.*

**4.3. Enforcing the Upper Bound Relation.** By definition, the polyconvex envelope  $\Phi^{\text{PC}}$  of the function  $\Phi$  is the largest polyconvex function below  $\Phi$ . Consequently, the goal is to ensure that the polyconvex envelopes predicted by the neural network are below the function  $\Phi$ . In what follows, we present different approaches and their limitations to achieving this. The direct approach to ensure the upper bound relation in the neural network, discussed in [Sections 4.3.1](#) and [4.3.2](#), is to integrate constraints in the architecture, while a weak approach is to penalise the loss function as discussed in [Section 4.3.3](#).

**4.3.1. Multiplication Layer.** One possible way to enforce the upper bound relation is to add a layer in the architecture which performs a multiplication operation. In this case, the output layer of the usual neural network consists in a neuron with an activation function  $g$  whose image lies between 0 and 1. Then, the modified output is calculated via a so-called multiplication layer, which performs the product of this last quantity and the values of the function  $\Phi$ , thereby guaranteeing that the prediction lies below the function  $\Phi$ . However, such a function  $g$  is often nonconvex, which causes nonconvexity of the overall network.

**4.3.2. Minimum Operation Layer.** Another possible way to enforce the upper bound relation is to add a layer in the architecture which performs a minimum operation, i.e. the final output is derived by taking the pointwise minimum between the predicted output and the value of the function  $\Phi$ , i.e.  $\min\{\Phi_{\text{pred},i}^{\text{PC}}, \Phi_i\}$ , where the subscript  $i$  denotes the evaluation of these functions at the  $i$ th learning input data point given as tuple of the form  $(m(\hat{\nu}), \zeta)$ . However, numerical experiments have shown that this constraint is too restrictive. Indeed, if the prediction is already below the function  $\Phi$ , then the model stops to learn.

**4.3.3. Penalisation via Loss Function.** Instead of adding constraints directly in the architecture, the upper bound relation can be imposed in a weak sense by penalisation. To achieve this, a custom loss function is designed, which penalises more severely if the prediction of the neural network is above the function  $\Phi$  during the training process. By minimising this loss function, the network should ultimately achieve predictions below  $\Phi$ . The loss function is thus written as

$$(14) \quad \mathcal{L} = \mathcal{L}_{\text{mse}} + \lambda_{\text{ineq}} \mathcal{L}_{\text{ineq}}$$

with

$$\mathcal{L}_{\text{mse}} = \frac{1}{N} \sum_{i=1}^N (\Phi_i^{\text{pc}} - \Phi_{\text{pred},i}^{\text{pc}})^2,$$

the classical mean square error, and

$$\mathcal{L}_{\text{ineq}} = \sum_{i=1}^N \max\{\Phi_{\text{pred},i}^{\text{pc}} - \Phi_i, 0\}^2,$$

where  $N$  is the size of the learning data,  $\Phi_{\text{pred}}^{\text{pc}}$  is the neural network prediction of the polyconvex envelope, and  $\Phi^{\text{pc}}$  is the target value to be approximated. The subscript  $i$  denotes the evaluation of these functions at the  $i$ th learning input data point given as tuple of the form  $(m(\hat{\nu}), \zeta)$ . The parameter  $\lambda_{\text{ineq}} \geq 0$  is the so-called penalty parameter, which determines how the two terms are weighted against each other and determines how strongly the network should be penalised if the prediction lies above  $\Phi$ . In this work, we used this strategy which has the advantage of not being intrusive, i.e. no modification of the neural network architecture is required.

**4.4. Enforcing the  $\Pi_d$ -Symmetry.** The function  $\Phi$  from (10) is subject to the invariance of  $\Pi_d$ , and the same holds for  $\Phi^{\text{pc}}$  from (12), that is it holds

$$\Phi^{\text{pc}}(\pi(\hat{\nu})) = \Phi^{\text{pc}}(\hat{\nu})$$

for all  $\pi \in \Pi_d$ , as discussed in Section 3. Consequently, this symmetry should be preserved by a neural network approximation.

As for the upper bound relation in Section 4.3.3, the symmetry of the prediction can be imposed in a weak sense by penalisation. To achieve this, a custom loss function which penalises more severely if the prediction of the neural network is not symmetric during the training process is designed. By minimising this loss function, the network should ultimately achieve symmetric predictions. Building upon the previously defined loss function (14) (keeping the same notations), already facilitating the upper bound relation, we add a term for the penalisation of the non-symmetry, leading to the loss function defined by

$$(15) \quad \mathcal{L} = \mathcal{L}_{\text{mse}} + \lambda_{\text{ineq}} \mathcal{L}_{\text{ineq}} + \lambda_{\text{sym}} \mathcal{L}_{\text{sym}}$$

with

$$\mathcal{L}_{\text{sym}} = \frac{1}{\#\Pi_d - 1} \sum_{\pi \in \Pi_d} \frac{1}{N} \sum_{i=1}^N \left( \Phi_{\text{pred},i}^{\text{pc}}(\hat{\nu}) - \Phi_{\text{pred},i}^{\text{pc}}(\pi(\hat{\nu})) \right)^2,$$

where the normalisation constant is motivated by the fact that the term corresponding to  $\pi = \text{id}$  does not contribute to the overall loss. The parameter  $\lambda_{\text{sym}} \geq 0$  is the penalty parameter, which determines how strongly the network should be penalised if the network is not symmetric with respect to the inputs. In addition, symmetry is further fostered by data augmentation. We incorporate symmetric data in the dataset, i.e. for a given point  $\hat{\nu}$ , the points  $\pi(\hat{\nu})$  for  $\pi \in \Pi_d$  are also included in the dataset.

**Remark 4.4** (Symmetry a posteriori). *The symmetry can also be enforced a posteriori, see for example [GKWM25], in which the symmetry is realised by averaging over all input permutations in the symmetry group*

$$\bar{\Phi}_{\text{pred}}^{\text{pc}}(\hat{\nu}) = \frac{1}{\#\Pi_d} \sum_{\pi \in \Pi_d} \Phi_{\text{pred}}^{\text{pc}}(\pi(\hat{\nu})).$$

*This method has the advantage of ensuring output symmetry in  $\bar{\Phi}_{\text{pred}}^{\text{pc}}$  without modifying the neural network architecture. However, this requires multiple evaluations of  $\Phi_{\text{pred}}^{\text{pc}}$  and the approximation  $\Phi_{\text{pred}}^{\text{pc}}$  is not necessarily symmetric.*

**4.5. Implementation and Hyperparameters.** The neural network architectures are implemented using PyTorch, and all the trainings are performed on an Intel<sup>®</sup> Core<sup>™</sup> i7-8700 machine, using only one core at a base frequency of 3.20 GHz.

The input data of the neural networks consist of the minors  $m(\hat{\nu}) \in \mathbb{R}^{k_d}$  of the signed singular values  $\hat{\nu}$  along with additional parameters  $\zeta \in \mathbb{R}^p$  depending on the definition of the function  $\Phi$ , i.e. the input data consists of vectors  $(m(\hat{\nu}), \zeta) \in \mathbb{R}^{k_d+p}$ . The target values correspond to the evaluation of the polyconvex envelope  $\Phi^{\text{pc}}$  at the points  $\hat{\nu}$  and the parameters  $\zeta$ , expressed as  $\Phi^{\text{pc}}(\hat{\nu}; \zeta)$ . In summary, the learning data (gathering both training and validation data) consists of tuples of the form  $(m(\hat{\nu}), \zeta, \Phi^{\text{pc}}(\hat{\nu}; \zeta), \Phi(\hat{\nu}; \zeta))$  containing the input features, the target value  $\Phi^{\text{pc}}(\hat{\nu}; \zeta)$ , and the value of the function  $\Phi(\hat{\nu}; \zeta)$ , which is necessary for the evaluation of the loss function (15).

In all the numerical examples, we design the neural network architectures to be as small as possible while maintaining high predictive accuracy. Indeed, preliminary numerical experiments have shown that increasing the number of layers or neurons of the neural networks presented below does not necessarily improve prediction performance; on the contrary, it may even degrade them. Also, we aim to use the smallest dataset size that ensures accurate predictions, while making training computationally efficient and feasible on a standard laptop, which has been achieved thanks to several investigations. We employ the ReLU activation function in all hidden layers, as it satisfies the convexity condition required by ICNN. The output layer consists of a single neuron with a linear activation function. Numerical experiments indicate that selecting ReLU as the convex activation function enhances learning efficiency and improves predictive accuracy compared to the Softplus function, another commonly employed activation function in ICNNs. Besides, [CSZ19, HCTC21] prove universal approximation theory of PICNN when ReLU, as well as Softplus, activation functions are used.

The weights  $W^{(z)}$  which belong to the convex part of the network are initialised from a normal distribution  $\mathcal{N}(0.1, 0.1)$  with 0.1 mean and 0.1 standard deviation, and then projected onto  $\mathbb{R}_+$ . Also, after each training step, the weights  $W^{(z)}$  are projected onto the  $\mathbb{R}_+$  halfspace to ensure their positiveness. This projection, essentially to ensure the positivity of the weights, is a crucial step. The naive application of ReLU for weight clipping can result in zero entries in the weight matrices and would waste approximation potential. For this projection, a shifted version of ReLU, i.e.  $x \rightarrow \max(x, 0) + \varepsilon$  with the small offset  $\varepsilon = 10^{-6}$  is employed. This initialisation and projection strategy has shown better performance compared to a uniform distribution, and projections using exponential or Softplus functions. The other weights are initialised from a uniform distribution  $\mathcal{U}(-1/\sqrt{n}, 1/\sqrt{n})$  with  $n$  the input size and all the biases are initialised to 0.

We employ the ADAMAX optimiser with a learning rate of  $\eta = 0.001$ , a batch size of 128, with the data shuffled at each epoch to improve model generalisation, and a patience of 10, i.e. the training process is stopped if no improvement of the validation error is achieved for 10 successive epochs. The training and validation errors are computed with the loss function (15). The hyperparameters  $\lambda_{\text{ineq}}$  and  $\lambda_{\text{sym}}$  involved in  $\mathcal{L}$  have been determined by performing several preliminary tests with different parameter values for  $\lambda_{\text{ineq}}$  and  $\lambda_{\text{sym}}$ . In each numerical example presented below, the given values of the  $(\lambda_{\text{ineq}}, \lambda_{\text{sym}})$  achieved the best training performance and predictions.

To obtain more reliable numerical results, for each example, we conduct ten runs of training, using the same training and validation data. The variations arise solely from the initialisation of model weights and the stochastic nature of data loading during training, since a shuffle is used. The numerical results presented are obtained by averaging the outputs of the ten network realisations.

## 5. MATHEMATICAL BENCHMARK EXAMPLES

To show the potential of the introduced approximation approaches by the property-preserving neural networks as introduced Section 4, we consider well-known examples in the context of

relaxation algorithms. Throughout all of the numerical experiments, we denote the analytical polyconvex envelope by  $\Phi^{\text{pc}}$  and by  $\Phi_{\text{pred}}^{\text{pc}}$  the neural network prediction.

**5.1. The Kohn–Strang–Dolzmann Function.** This function was studied in [KS86a, KS86b], subsequently modified to achieve continuity in [Do199, DW00] and further studied in [Bar05] and serves as a first benchmark example to illustrate the possibility of the neural network approach to approximate the polyconvex envelope. We consider the function  $W: \mathbb{R}^{2 \times 2} \rightarrow \mathbb{R}$ , defined as

$$W(F) = \begin{cases} 1 + |F|^2 & \text{if } |F| \geq \sqrt{2} - 1, \\ 2\sqrt{2}|F| & \text{else,} \end{cases}$$

where  $|F| := (\sum_{i,j=1}^d F_{ij}^2)^{1/2}$  denotes the Frobenius norm of the matrix  $F$ . The polyconvex envelope of  $W$  is explicitly known, see e.g. [Do199], and reads

$$W^{\text{pc}}(F) = \begin{cases} 1 + |F|^2 & \text{if } \rho(F) \geq 1, \\ 2(\rho(F) - |\det(F)|) & \text{else,} \end{cases}$$

where  $\rho(F) := \sqrt{|F|^2 + 2|\det(F)|}$ . The functions  $W$  and  $W^{\text{pc}}$  are isotropic; consequently, they can be rewritten in terms of the signed singular values and reduce to  $\Phi, \Phi^{\text{pc}}: \mathbb{R}^2 \rightarrow \mathbb{R}$  with

$$\Phi(\hat{\nu}) = \begin{cases} 1 + \nu_1^2 + \nu_2^2 & \text{if } \sqrt{\nu_1^2 + \nu_2^2} \geq \sqrt{2} - 1, \\ 2\sqrt{2}\sqrt{\nu_1^2 + \nu_2^2} & \text{else,} \end{cases}$$

and

$$(16) \quad \Phi^{\text{pc}}(\hat{\nu}) = \begin{cases} 1 + \nu_1^2 + \nu_2^2 & \text{if } \rho(\hat{\nu}) \geq 1, \\ 2(|\nu_1| + |\nu_2| - |\nu_1\nu_2|) & \text{else,} \end{cases}$$

where  $\rho(\hat{\nu}) = |\nu_1| + |\nu_2|$ .

**5.1.1. Network Architecture and Learning Data.** In this example, we implement a FICNN which consists of two hidden layers, with 10 and 20 neurons, respectively, as presented in [Figure 3](#). The learning domain for  $\hat{\nu}$  is defined as the box  $[-\bar{\nu}, \bar{\nu}]^2$  with  $\bar{\nu} = 1.05$ . For the training, the set of signed singular values  $\hat{\nu}$  used as input is generated by discretising each axis with 751 points, so that the point 0 is included, making  $751^2$  training data points in total. Instead of using a uniform distribution of the points, we use a local refinement towards the origin, utilising a quadratic transformation. This refinement approach increases the data density near the point of non-differentiability of both functions  $\Phi$  and  $\Phi^{\text{pc}}$ . For the validation dataset, we randomly sample 169,200 points within the domain  $[-\bar{\nu}, \bar{\nu}]^2$ , accounting for 30% of the training dataset size. The target values, i.e. the polyconvex envelope, are obtained by evaluation of the analytical function  $\Phi^{\text{pc}}$  as in (16). For the loss function, we choose the penalty parameters  $\lambda_{\text{ineq}} = 1.5$  and  $\lambda_{\text{sym}} = 1$ .

**5.1.2. Numerical Results.** On average, for a single realisation, the training process requires  $21 \pm 4$  minutes to complete  $77 \pm 17$  epochs. The final training error is  $1.47 \times 10^{-3} \pm 2.71 \times 10^{-4}$ , while the validation error reaches  $1.59 \times 10^{-3} \pm 3.45 \times 10^{-4}$ . The learning curves for both training and validation errors on one exemplary realisation are presented in [Figure 3](#).

Mean error	Rel. quadratic error	Rel. max error
$0.027 \pm 2.59 \times 10^{-3}$	$0.021 \pm 1.80 \times 10^{-3}$	$0.031 \pm 3.37 \times 10^{-3}$

TABLE 1. Average of prediction errors over ten network realisations.

[Table 1](#) presents the approximation errors of the predictions, where the analytical polyconvex envelope is used as a ground truth. These errors are computed on a uniform  $100 \times 100$  discretisation of the domain  $[-\bar{\nu}, \bar{\nu}]^2$ . The results indicate that the predicted envelopes deviate by about 2% to 3% from the analytical polyconvex envelope  $\Phi^{\text{pc}}$ , demonstrating an accuracy sufficient for the intended engineering applications. The approximation quality is further illustrated in [Figure 4](#),

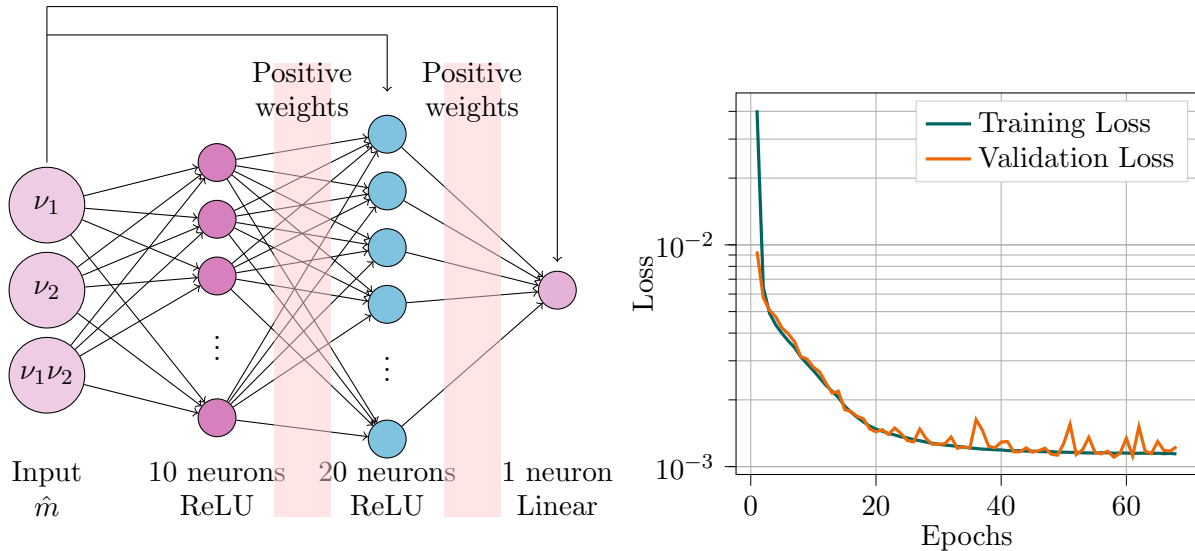


FIGURE 3. Left: Network architecture for Kohn–Strang–Dolzmann example. Right: Learning curves based on the loss function  $\mathcal{L}$  from (15) for a single network initialisation.

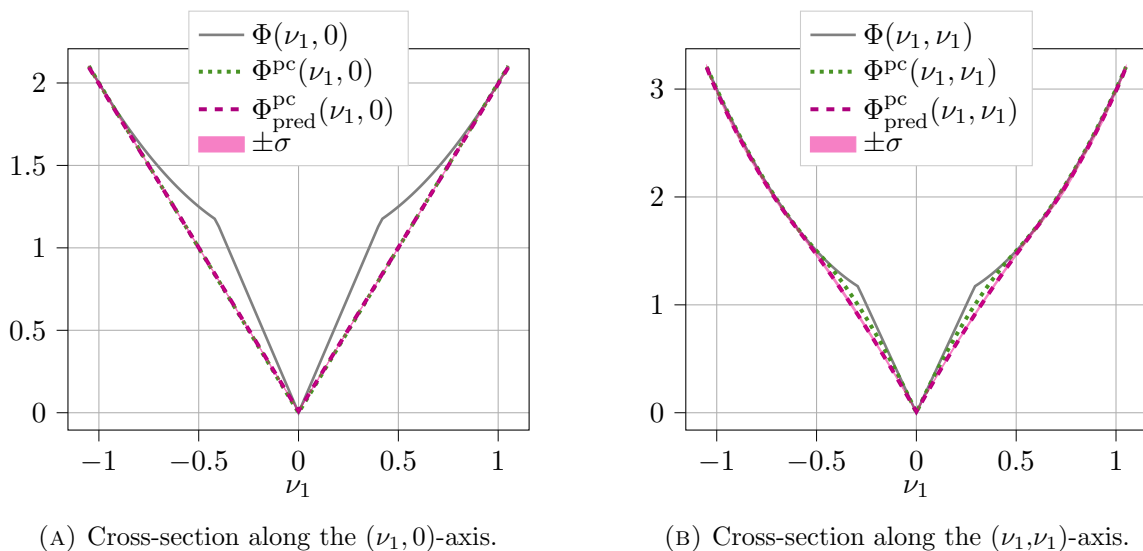


FIGURE 4. Comparison of the predicted polyconvex envelope  $\Phi_{\text{pred}}^{\text{PC}}$  (averaged over ten network realisations) and the analytical polyconvex envelope  $\Phi^{\text{PC}}$  for the Kohn–Strang–Dolzmann function along two cross-sections. The standard deviation of the ten predictions is marked by  $\sigma$ .

where two one-dimensional cross-sections of the predicted polyconvex envelope are depicted. It is important to note that the neural network successfully captures the kink of the function  $\Phi^{\text{PC}}$  at the point  $(0,0)$  with high accuracy. Further, it is notable that the neural network based approximation captures the nonconvexity along the diagonal cross-section of the envelope, rendering it a consistent polyconvex function. It is observable that the standard deviation  $\sigma$  of the different network realisations is quite negligible when it comes to the approximation accuracy. Specifically, the neural network implemented in this example contains 365 parameters, comprising both weights and biases. With the same number of parameters using the conventional approach, it would only be possible to store  $19 \times 19$  grid values, and then approximate the value at any point by interpolation. While this standard method remains feasible for simple cases, it can

quickly become intractable for more complex scenarios, such as parameter-dependent functions or real engineering problems.

**Remark 5.1.** *In addition to the values of the polyconvex envelopes, most engineering applications also require their derivatives. We briefly point out two straight forward approaches for predicting these derivatives. The first approach involves differentiating the predictions of the neural network directly using standard finite difference methods. However, preliminary results indicate that this method suffers from significant drawbacks owing to the lack of continuity in the network evaluations. A more conventional alternative is to train a separate neural network to learn the derivatives of the polyconvex envelopes. Initial numerical experiments on this example demonstrate that this can be achieved with a relatively simple network architecture, consisting of two hidden layers with 10 and 20 neurons, ReLU activation functions and a two-dimensional output with linear activation functions. However, we do not pursue this direction further as it is beyond the scope of this paper.*

**5.2. The Generalised Kohn–Strang–Dolzmann Function.** After the previous initial benchmark example, we consider a more complex case, i.e. a two-parameter-dependent family of functions. The following example was studied in [AF98, Zha02] and modified to achieve continuity. We consider the function  $W: \mathbb{R}^{2 \times 2} \times \mathbb{R}_+ \times \mathbb{R}_+ \setminus \{0\} \rightarrow \mathbb{R}$ , defined as

$$W(F; \lambda, \alpha) = \begin{cases} \lambda + \alpha |F|^2 & \text{if } |F| \geq \sqrt{\frac{\lambda}{\alpha}} (\sqrt{2} - 1), \\ 2\sqrt{2\lambda\alpha} |F| & \text{else,} \end{cases}$$

where  $|F| := (\sum_{i,j=1}^d F_{ij}^2)^{1/2}$ . The polyconvex envelope of  $W$  is known analytically in closed form and reads

$$W^{\text{pc}}(F; \lambda, \alpha) = \begin{cases} \lambda + \alpha |F|^2 & \text{if } \rho(F) \geq \sqrt{\frac{\lambda}{\alpha}}, \\ 2\sqrt{\lambda\alpha} \rho(F) - 2\alpha |\det(F)| & \text{else,} \end{cases}$$

where  $\rho(F) := \sqrt{|F|^2 + 2|\det(F)|}$ . The functions  $W$  and  $W^{\text{pc}}$  are isotropic, and, rewritten in terms of the signed singular values, they reduce to  $\Phi, \Phi^{\text{pc}}: \mathbb{R}^2 \times \mathbb{R}_+ \times \mathbb{R}_+ \setminus \{0\} \rightarrow \mathbb{R}$  with

$$(17) \quad \Phi(\hat{\nu}; \lambda, \alpha) = \begin{cases} \lambda + \alpha (\nu_1^2 + \nu_2^2) & \text{if } \sqrt{\nu_1^2 + \nu_2^2} \geq \sqrt{\frac{\lambda}{\alpha}} (\sqrt{2} - 1), \\ 2\sqrt{2\lambda\alpha} \sqrt{\nu_1^2 + \nu_2^2} & \text{else,} \end{cases}$$

and

$$(18) \quad \Phi^{\text{pc}}(\hat{\nu}; \lambda, \alpha) = \begin{cases} \lambda + \alpha (\nu_1^2 + \nu_2^2) & \text{if } \rho(\hat{\nu}) \geq \sqrt{\frac{\lambda}{\alpha}}, \\ 2\sqrt{\lambda\alpha} (|\nu_1| + |\nu_2|) - 2\alpha |\nu_1\nu_2| & \text{else,} \end{cases}$$

where  $\rho(\hat{\nu}) = |\nu_1| + |\nu_2|$ .

**5.2.1. Network Architecture and Learning Data.** For this parameter-dependent example, we implement a PICNN where each path consists of three hidden layers with 10, 20, and 20 neurons, respectively. The convex input, denoted by  $\hat{m}$ , represents the minors of the signed singular values, i.e.  $m(\hat{\nu})$ , while the nonconvex inputs, denoted as vector  $\zeta$ , correspond to the two parameters  $\lambda$  and  $\alpha$ . The learning domain for  $\hat{\nu}$  is defined as  $[-\bar{\nu}, \bar{\nu}]^2$  with  $\bar{\nu} = 1.05$ , while the learning domain is  $[1, 2]$  for each of the parameters  $\lambda$  and  $\alpha$ . For the training dataset, the set of points in the signed singular value space is obtained by discretising each axis into 201 points, so that the point 0 is included, with a local refinement towards the origin using a quadratic transformation, as in the previous example. The parameter  $\lambda$  takes values from the discrete set  $\{1, 1.2, \dots, 1.8, 2\}$  and  $\alpha$  follows the same parameter discretisation. These discretisations lead to a total of 1,454,436 points in the training dataset. For the validation dataset, in the parameter components we randomly select six values each for  $\lambda$  and for  $\alpha$  within the interval  $[1, 2]$ , and for each couple of parameters  $(\lambda, \alpha)$  we randomly sample  $130^2$  points in the  $\nu$  argument within the domain  $[-\bar{\nu}, \bar{\nu}]^2$ , making hence 608,400 points. Consequently, the training dataset accounts for 70% of the total learning dataset, while the validation dataset accounts for 30% of it. The target values are computed using the analytical function  $\Phi^{\text{pc}}$ , cf. (18). **Figure 5** illustrates a one-dimensional

representation of the target values for the training dataset along the diagonal  $(\nu_1, \nu_1)$ -axis. For the loss function  $\mathcal{L}$  from (15), we choose the penalty parameters  $\lambda_{\text{ineq}} = 1.5$  and  $\lambda_{\text{sym}} = 1$ .

5.2.2. *Numerical Results.* On average, for a single realisation, the training process requires  $3.6 \text{ h} \pm 54 \text{ minutes}$  to complete  $87 \pm 22$  epochs. The final training error is  $2.31 \times 10^{-3} \pm 1.62 \times 10^{-3}$ , while the validation error reaches  $3.53 \times 10^{-3} \pm 2.29 \times 10^{-3}$ . The learning curves for one selected realisation are plotted in Figure 5.

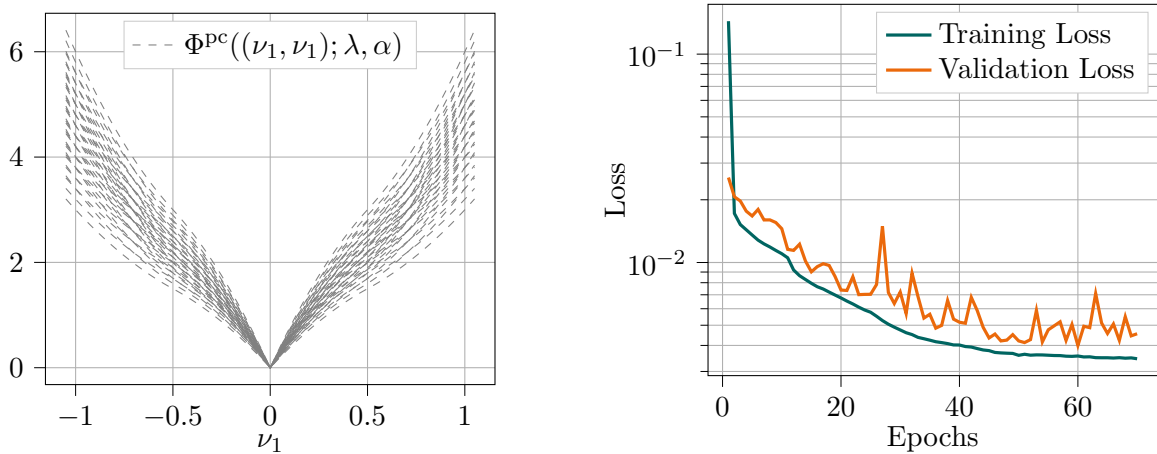


FIGURE 5. Left: Training data for the generalised Kohn–Strang–Dolzmann example. One-dimensional cross-section along the diagonal  $(\nu_1, \nu_1)$ -axis of the analytical polyconvex envelopes. Envelopes are evaluated at the training points in parameter space, i.e. for  $(\lambda, \alpha) \in \{1, 1.2, \dots, 1.8, 2\}^2$ . Right: Learning curves based on the loss function  $\mathcal{L}$  from (15) for a single network initialisation.

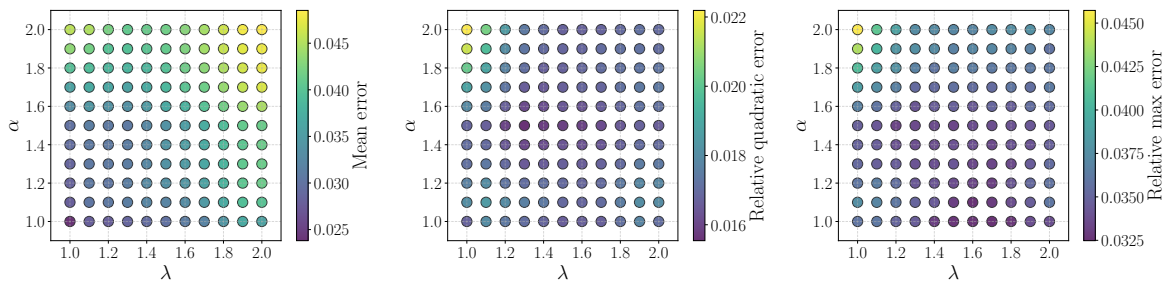


FIGURE 6. Errors over parameter space for the generalised Kohn–Strang–Dolzmann example. Left: Mean errors. Middle: Relative quadratic errors. Right: Relative max errors. All errors are computed for an average over ten network realisations with respect to the analytical polyconvex envelopes for different values  $\lambda$  and  $\alpha$ .

Figure 6 illustrates the relative errors between the predictions and the analytical polyconvex envelopes for different sets of parameters  $(\lambda, \alpha)$ , including both values present in the training set and those outside of it. These errors are computed on a uniform  $(100 \times 100)$ -discretisation of the domain  $[-\bar{\nu}, \bar{\nu}]^2$ . Across all considered parameter sets, the errors remain consistently low, ranging between 2% and 4%. Additionally, Figure 7 provides one-dimensional cross-sections of these predictions. Furthermore, Figure 8 demonstrates that the neural network is capable of making accurate predictions even for parameter values outside the parameter learning domain, highlighting its ability to extrapolate accurately. Notably, these figures indicate that errors are primarily localised at the domain boundaries, while the neural network successfully captures the kink at the point  $(0, 0)$  with an accuracy sufficient for most engineering applications. In

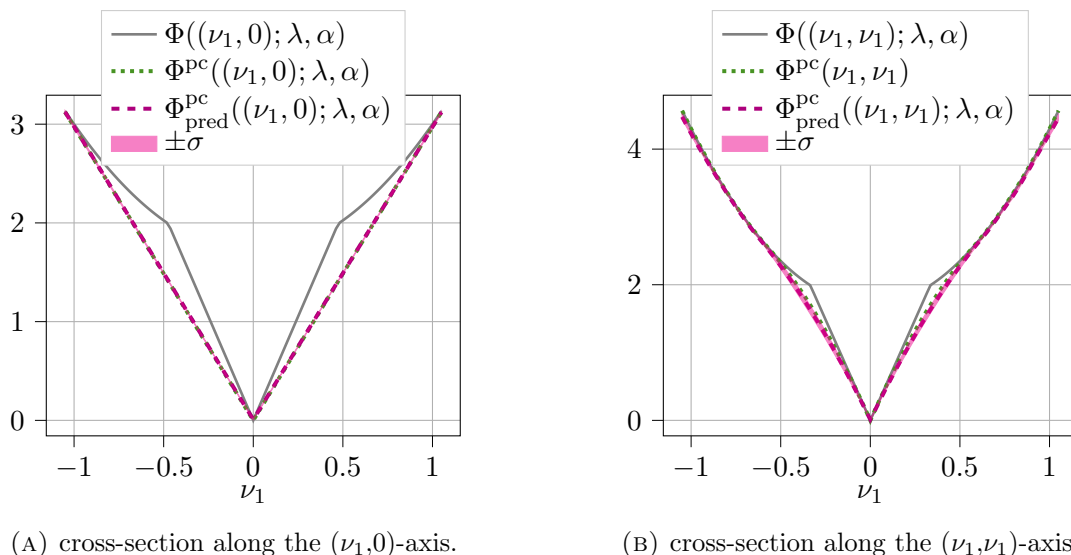


FIGURE 7. Comparison along two axes of the predicted polyconvex envelope  $\Phi_{\text{pred}}^{\text{PC}}$  (averaged over ten network realisations) and the analytical polyconvex envelope  $\Phi^{\text{PC}}$  for the Generalised Kohn–Strang–Dolzmann function with  $\lambda = 1.7$  and  $\alpha = 1.3$ . The standard deviation of the ten predictions is marked by  $\sigma$ .

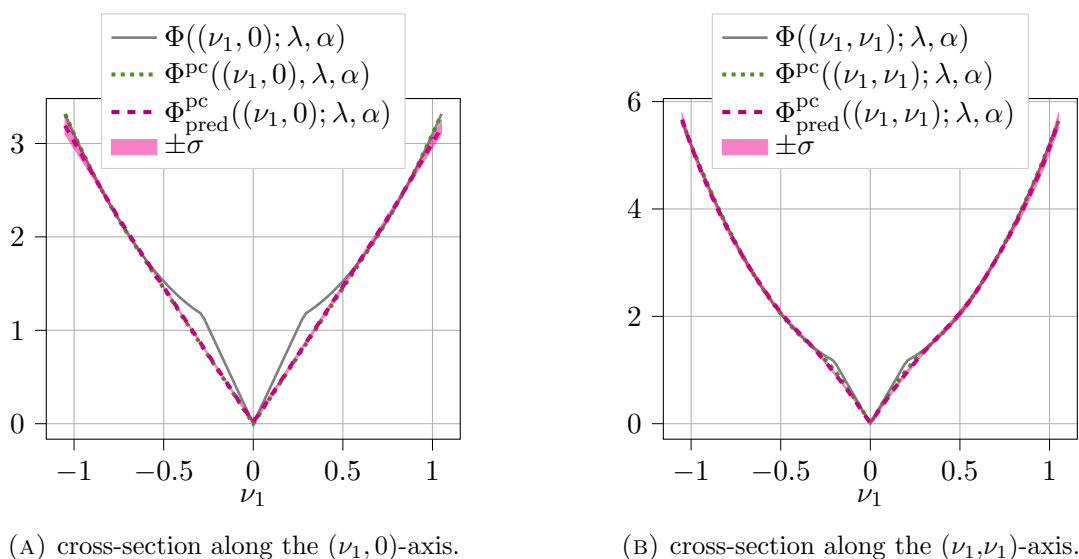


FIGURE 8. Comparison along two axes of the predicted polyconvex envelope  $\Phi_{\text{pred}}^{\text{PC}}$  (averaged over ten network realisations) and the analytical polyconvex envelope  $\Phi^{\text{PC}}$  for the Generalised Kohn–Strang–Dolzmann function with  $\lambda = 1$  and  $\alpha = 2.1$ , these parameters are located outside the parameter learning domain. The standard deviation of the ten predictions is marked by  $\sigma$ .

particular, the neural network implemented in this example contains 3344 parameters, comprising both weights and biases. With the same number of parameters using the conventional approach, it would only be possible to store a  $19 \times 19$  grid, with 3 values for each  $\lambda$  and  $\alpha$ . With this limited grid size, it is evident that the full range of data cannot be recovered with the same precision as is achievable with neural networks presented here.

## 6. ENGINEERING EXAMPLE: ISOTROPIC DAMAGE PROBLEM

Having validated our approach with mathematical benchmark problems, we return to the isotropic damage problem introduced in Section 2. In order to fit this model into our setting, we rephrase it in signed singular value formulation.

**6.1. Reformulation of the Isotropic Damage Problem.** The function  $W$  from (4) is dependent on  $d \times d + 1$  parameters and on the  $d \times d$ -deformation gradient. Due to the isotropy of  $W$ , it can be recast into a signed singular value formulation utilising  $\hat{\nu} \in \mathbb{R}^d$ . To stress the dependence on the signed singular values, the function  $\varphi$  is now employed to rewrite (5) as

$$\varphi(\hat{\nu}, \alpha) = (1 - D(\alpha)) \varphi^0(\hat{\nu}).$$

Within this formulation, the function  $\varphi^0$  denotes the signed singular value formulation of the isotropic undamaged energy density  $\psi^0$  from (5), i.e.  $\varphi^0$  and  $\psi^0$  are related by

$$\varphi^0(\hat{\nu}) = \psi^0(\text{diag}(\hat{\nu})) \quad \text{and} \quad \psi^0(F) = \varphi^0(\nu(F)).$$

Consequently, the pseudo-time incremental energy density  $W$  in the signed singular value formulation, denoted by  $\Phi$ , for the time step  $k + 1$  reads

$$(19) \quad \begin{aligned} \Phi(\hat{\nu}_{k+1}; \hat{\nu}_k, \alpha_k) &= \varphi(\hat{\nu}_{k+1}, p(\hat{\nu}_{k+1}; \alpha_k)) - \varphi(\hat{\nu}_k, \alpha_k) \\ &+ p(\hat{\nu}_{k+1}; \alpha_k) D(p(\hat{\nu}_{k+1}; \alpha_k)) - \alpha_k D(\alpha_k) - \bar{D}(p(\hat{\nu}_{k+1}; \alpha_k)) + \bar{D}(\alpha_k). \end{aligned}$$

The parameter dependence in this function can be given the following interpretation. The scalar parameter  $\alpha_k$  plays still the same role as the internal variable, while the vector  $\hat{\nu}_k \in \mathbb{R}^d$  belongs to the signed singular values of the deformation gradient  $F_k$  from the previous pseudo-time step. Within (19), the internal variable evolution is written explicitly using the path function in the signed singular value formulation as

$$(20) \quad \alpha_{k+1} = p(\hat{\nu}_{k+1}; \alpha_k) = \begin{cases} \varphi^0(\hat{\nu}_{k+1}) & \text{if } \varphi^0(\hat{\nu}_{k+1}) > \alpha_k, \\ \alpha_k & \text{else.} \end{cases}$$

The formulation as stated in (19) significantly reduces dimensionality in both the  $\hat{\nu}_{k+1}$  argument as well as the  $\hat{\nu}_k$  parameter dependence, opening the possibility for efficient parameter-dependent polyconvexification of the function  $\Phi(\hat{\nu}_{k+1}; \hat{\nu}_k, \alpha_k)$  in the argument  $\hat{\nu}_{k+1}$ . For the neural network, this leads to a reduction in parameter space from  $d \times d + 1$  to  $d + 1$  dimensions, and a reduction in the minors input argument from dimension  $K_d$  to  $k_d$ , corresponding to the dimension of the vector  $m(\hat{\nu}_{k+1})$ .

The damage parameters  $d_0$  and  $d_\infty$  are set to  $d_0 = 0.5$ ,  $d_\infty = 0.99$  in our numerical experiments. The Lamé constants  $\lambda$  and  $\nu$  of the materials in (2) and (3) are set to  $\lambda = 0$ ,  $\mu = 0.5$ .

**Remark 6.1.** *Let us consider  $\alpha_\infty$  and  $k_0$  such that for all  $k \geq k_0$  it holds  $\alpha_k \geq \alpha_\infty$  and by evolution it holds  $\alpha_{k+1} \geq \alpha_k$ . For the choice of damage function  $D$  in (6), we have for  $\alpha_\infty$  large enough that  $D(\alpha_k) \approx d_\infty$  and  $\bar{D}(\alpha_k) \approx \alpha_k d_\infty$  for  $d_\infty$  marking the asymptotic damage limit. In such a case, (19) can be rewritten as*

$$\begin{aligned} \Phi(\hat{\nu}_{k+1}; \hat{\nu}_k, \alpha_k) &\approx (1 - d_\infty) \varphi^0(\hat{\nu}_{k+1}) - (1 - d_\infty) \varphi^0(\hat{\nu}_k) \\ &\quad + \alpha_{k+1} d_\infty - \alpha_k d_\infty - \alpha_{k+1} d_\infty + \alpha_k d_\infty \\ &\approx (1 - d_\infty) (\varphi^0(\hat{\nu}_{k+1}) - \varphi^0(\hat{\nu}_k)). \end{aligned}$$

Consequently, for  $\alpha_k \geq \alpha_\infty$ , the energy becomes independent of  $\alpha_k$ . This observation allows to train the neural network for the parameter  $\alpha_k \in [0, \alpha_\infty]$  and to consider  $\alpha_k = \alpha_\infty$  for the predictions in the case  $\alpha_k \geq \alpha_\infty$ , which drastically reduces the computational effort. For the choice of parameters  $d_0$  and  $d_\infty$ , we choose  $\alpha_\infty = 4$  in the numerical experiments noting that for  $\alpha_k \geq \alpha_\infty$ , we can perform the estimate

$$|D(\alpha_\infty) - D(\alpha_k)| \leq \left| \exp\left(-\frac{\alpha_\infty}{d_0}\right) - \exp\left(-\frac{\alpha_k}{d_0}\right) \right| \leq \exp\left(-\frac{\alpha_\infty}{d_0}\right) = \exp(-8) \approx 3 \times 10^{-4},$$

which is much smaller than the prediction accuracy of the neural networks. This choice is also motivated by numerical experiments.

**6.2. Normalisation by a Splitting Approach.** At this stage, the incremental energy density  $\Phi$  depends on  $d + 1$  parameters and shows significant variation over the parameter domain  $\hat{\nu}_k$  and  $\alpha_k$ . This pronounced separation between function curves is a challenge for neural networks as it hinders efficient learning. Large gaps between function values can prevent smooth interpolation and generalisation, making it difficult to capture underlying patterns during training - unless a large amount of data is used, which becomes intractable even in two spatial dimensions. Although  $\Phi$  depends only on  $d + 1$  parameters, the parameter  $\hat{\nu}_k$  requires a discretisation as fine as the discretisation for the argument  $\hat{\nu}_{k+1}$  since they play a similar role, making the learning computationally infeasible.

To overcome these difficulties, we take advantage of the structure of the pseudo-time incremental energy density function. The function  $\Phi$  from (19) can be expressed as

$$\Phi(\hat{\nu}_{k+1}; \hat{\nu}_k, \alpha_k) = \tilde{\Phi}(\hat{\nu}_{k+1}; \alpha_k) + \Phi_{\text{shift}}(\hat{\nu}_k, \alpha_k),$$

where  $\tilde{\Phi}: \mathbb{R}^d \times \mathbb{R} \rightarrow \mathbb{R}_\infty$  and  $\Phi_{\text{shift}}: \mathbb{R}^d \times \mathbb{R} \rightarrow \mathbb{R}_\infty$  are defined as

$$(21) \quad \begin{aligned} \tilde{\Phi}(\hat{\nu}_{k+1}; \alpha_k) := & \varphi(\hat{\nu}_{k+1}, p(\hat{\nu}_{k+1}; \alpha_k)) \\ & + p(\hat{\nu}_{k+1}; \alpha_k) D(p(\hat{\nu}_{k+1}; \alpha_k)) - \alpha_k D(\alpha_k) - \bar{D}(p(\hat{\nu}_{k+1}; \alpha_k)) + \bar{D}(\alpha_k) \end{aligned}$$

and

$$\Phi_{\text{shift}}(\hat{\nu}_k, \alpha_k) := -\varphi(\hat{\nu}_k, \alpha_k),$$

respectively. It should be stressed that the function  $\Phi_{\text{shift}}$  is independent of  $\hat{\nu}_{k+1}$ , hence only dependent on the parameters and constant in the convexification argument  $\hat{\nu}_{k+1}$ . Assuming the function  $\varphi^0$  is normalised in the sense that  $\inf_{\hat{\nu}} \varphi^0(\hat{\nu}) = \varphi^0(\mathbb{1}_d) = 0$ , the function  $\tilde{\Phi}$  is also normalised, i.e.  $\inf_{\hat{\nu}_{k+1}} \tilde{\Phi}(\hat{\nu}_{k+1}; \alpha_k) = \tilde{\Phi}(\mathbb{1}_d) = 0$ , where  $\mathbb{1}_d \in \mathbb{R}^d$  denotes the vector containing only ones. Consequently, the polyconvex envelope of  $\Phi$  can be obtained from the polyconvexification of the function  $\tilde{\Phi}$  by

$$(22) \quad \Phi^{\text{PC}}(\hat{\nu}_{k+1}; \hat{\nu}_k, \alpha_k) = \tilde{\Phi}^{\text{PC}}(\hat{\nu}_{k+1}; \alpha_k) + \Phi_{\text{shift}}(\hat{\nu}_k, \alpha_k).$$

Therefore,  $\tilde{\Phi}^{\text{PC}}$  should be the focus of an approximation by a neural network or a standard algorithm. Note that this normalisation is domain independent, and just relies on the split (22), considering the contribution  $\Phi_{\text{shift}}$  as a shift. Removing the dependence on the previous time step  $\hat{\nu}_k$  reduces the polyconvexification problem to a one-parameter-dependent family, making the learning feasible. In what follows, the neural networks are trained to predict the function  $\tilde{\Phi}^{\text{PC}}$  and the function  $\Phi^{\text{PC}}$  is recovered a posteriori by applying the shift  $\Phi_{\text{shift}}$  as stated in (22).

**6.3. Numerical Approximation of the Polyconvex Envelope.** For the isotropic damage model considered in this section, i.e.  $\Phi$  from (19), there is no closed form analytical formulation of the polyconvex envelope available. This is why, for the computation of the target values the polyconvex envelopes are approximated numerically utilising the algorithm for isotropic functions based on a linear programming approach presented in [NPPW24]. For this approximation procedure, the pointwise characterisation of the polyconvex envelope  $\Phi^{\text{PC}}$  at  $\hat{\nu} \in \mathbb{R}^d$  by the optimisation problem

$$(23) \quad \Phi^{\text{PC}}(\hat{\nu}) = \inf \left\{ \sum_{i=1}^{k_d+1} \xi_i \Phi(\nu_i) \mid \xi_i \in [0, 1], \nu_i \in \mathbb{R}^d, \sum_{i=1}^{k_d+1} \xi_i = 1, \sum_{i=1}^{k_d+1} \xi_i m(\nu_i) = m(\hat{\nu}) \right\}$$

is employed. For an algorithmic approximation of this problem, consider a discretisation of the signed singular value space by a point cloud, denoted by  $\Sigma_\delta = \{\nu_1, \dots, \nu_{N_\delta}\} \subset \mathbb{R}^d$ , a possible choice is the structured lattice  $\Sigma_\delta = \delta \mathbb{Z}^d \cap [-r, r]^d$ , for lattice size  $\delta$  and discretisation radius  $r$ . The lifting of this point cloud  $m(\Sigma_\delta)$  can be employed to turn the nonlinear optimisation problem (23) into the following linear program

$$(24) \quad \Phi_\delta^{\text{PC}}(\hat{\nu}) = \min \left\{ \sum_{i=1}^{N_\delta} \xi_i \Phi(\nu_i) \mid \xi_i \geq 0, \sum_{i=1}^{N_\delta} \xi_i = 1, \sum_{i=1}^{N_\delta} \xi_i m(\nu_i) = m(\hat{\nu}) \right\},$$

which can be efficiently solved numerically using standard algorithms for linear programming. The overall procedure is referred to as signed singular value polyconvexification by linear programming

(SVPC LP). In exact arithmetics, there exists a minimiser  $\xi \in \mathbb{R}^{N_\delta}$  of (24) with at most  $k_d + 1$  non-zero entries reflecting the convex coefficients of the supporting points of the polyconvex envelope at  $\hat{\nu}$  in the set  $\Sigma_\delta$  which are sometimes also referred to as volume fractions. For a detailed description of the algorithm see [NPPW24], a MATLAB implementation can be found under <https://github.com/TmNmr/SVPC>. In this paper, we use a python implementation of this algorithm which uses the `scipy.optimize.linprog` function for solving the linear program.

In the numerical examples, the structured lattice for the algorithm is obtained by discretising uniformly the learning domain for  $\hat{\nu}_{k+1}$ , i.e.  $[\nu_{\min}, \nu_{\max}]^d$  with 256 points along each axis leading to a lattice  $\Sigma_\delta$  consisting of  $N_\delta = 256^d$  points. For this choice of discretisation size  $\delta$ , an absolute error compared to the analytical polyconvex envelope of order  $10^{-5}$  can be predicted, see e.g. [NPPW24, Figures 4.2, 4.4 and 4.5]. In what follows, we denote by  $\tilde{\Phi}_\delta^{\text{pc}}$  the approximation of the polyconvex envelope by the SVPC LP algorithm.

**6.4. Numerical Results for the Two-Dimensional Saint Venant–Kirchhoff Model.** We consider the function  $\Phi$  from (19) in the Saint Venant–Kirchhoff-based formulation, i.e.  $\psi^0$  from (2) is chosen with the material parameters as before. We aim for the representation of the function  $\tilde{\Phi}^{\text{pc}}: \mathbb{R}^d \times \mathbb{R}_+ \rightarrow \mathbb{R}$ , i.e. the polyconvex envelope of the normalised version (21), by a neural network.

**6.4.1. Network Architecture and Learning Data.** In this example, we implement a PICNN where each path consists of three hidden layers with 30, 60, and 60 neurons, respectively. The convex input, denoted as  $\hat{m}$ , represents the minors of the signed singular values  $\hat{\nu}_{k+1}$ , i.e.  $m(\hat{\nu}_{k+1})$ , while the nonconvex inputs, denoted as  $\zeta$ , correspond to the parameter  $\alpha_k$ . The learning domain for  $\hat{\nu}_{k+1}$  is defined as  $[\nu_{\min}, \nu_{\max}]^2$  with  $\nu_{\min} = 0.001$  and  $\nu_{\max} = 5$ , while the learning domain for the parameter  $\alpha_k$  is  $[0, \alpha_\infty]$ . For the learning dataset, the set of points in the signed singular value space is obtained by discretising each axis as follows,  $[\nu_{\min} : 0.005 : 1] \cup [1 : 0.015 : \nu_{\max}]$ , leading to a  $464 \times 464$  grid, and we choose the set of learning values  $\alpha_k$  as  $\mathcal{I}_{\alpha_k} = \{0, 0.1, \dots, 1.5, 1.7, 2, 2.5, 3, 3.5, 4\}$ , i.e. 22 values. These discretisations lead to a learning dataset size of 4,736,512 points. From this dataset, 70% of the samples are randomly assigned to the training set, while the remaining 30% constitute the validation set. The target values  $\tilde{\Phi}_\delta^{\text{pc}}$  are computed with the SVPC LP algorithm. The computation of the target values takes 3510 CPU hours. Figure 9 illustrates the target values along the axis  $(\nu_1, \nu_1)$ . For the loss function, we choose the penalty parameters  $\lambda_{\text{ineq}} = 1$  and  $\lambda_{\text{sym}} = 1$ .

**6.4.2. Numerical Results.** On average, for a single realisation, the training process requires  $2.23 \text{ h} \pm 30 \text{ minutes}$  to complete  $54 \pm 12$  epochs. The final training error is  $5.10 \times 10^{-5} \pm 6.09 \times 10^{-6}$ , while the validation error reaches  $4.21 \times 10^{-5} \pm 1.27 \times 10^{-5}$ . The learning curves for one of these realisations are presented in Figure 9.

Figure 10 illustrates the relative errors between the predictions and the polyconvex envelopes computed by the algorithm from Section 6.3 for different values of  $\alpha_k$ , including values that are outside the training domain. These errors are computed on a uniform  $100 \times 100$  lattice of the domain  $[\nu_{\min}, \nu_{\max}]^2$ . Across all considered values  $\alpha_k$ , the errors remain consistently low, ranging between 1% and 2%. In particular, it is important to note that the hypothesis stating that the energies become independent from  $\alpha_k$  for  $\alpha_k \geq \alpha_\infty$  is verified and validates the choice of  $\alpha_\infty = 4$ .

Additionally, Figure 11 provides examples of re-shifted predictions which are in good agreement with the polyconvex envelopes computed by the SVPC LP algorithm. Specially, these predictions are obtained for values of  $\alpha_k$  that are not included in the learning set  $\mathcal{I}_{\alpha_k}$  and lie outside the parameter’s training domain, demonstrating good predictability and generalisation capabilities of the network.

For comparison, the computation of one polyconvex envelope on a  $(100 \times 100)$ -grid using the SVPC LP algorithm of Section 6.3 takes 7.2 hours on one CPU while its prediction via neural networks takes only 0.2 seconds, emphasising once again the benefits of using a neural network approach for polyconvexification in engineering applications. In addition, the neural network implemented in this example contains 26,121 parameters, comprising both weights and biases.

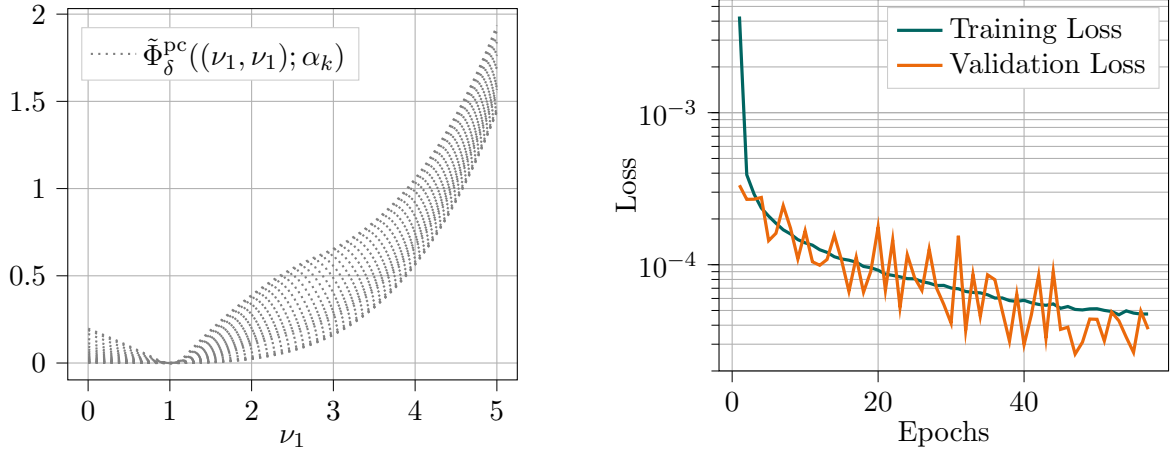


FIGURE 9. Left: Learning data for STVK based damage. Diagonal cross-sections of the target values, i.e. polyconvex envelopes  $\tilde{\Phi}_\delta^{\text{pc}}$  for the Saint Venant–Kirchhoff-based function  $\tilde{\Phi}$  with  $\alpha_k \in \mathcal{I}_{\alpha_k}$ . Right: Learning curves for STVK based damage. Learning curves based on  $\mathcal{L}$  from (15) for a single network initialisation for the Saint Venant–Kirchhoff-based function  $\tilde{\Phi}_\delta^{\text{pc}}$ .

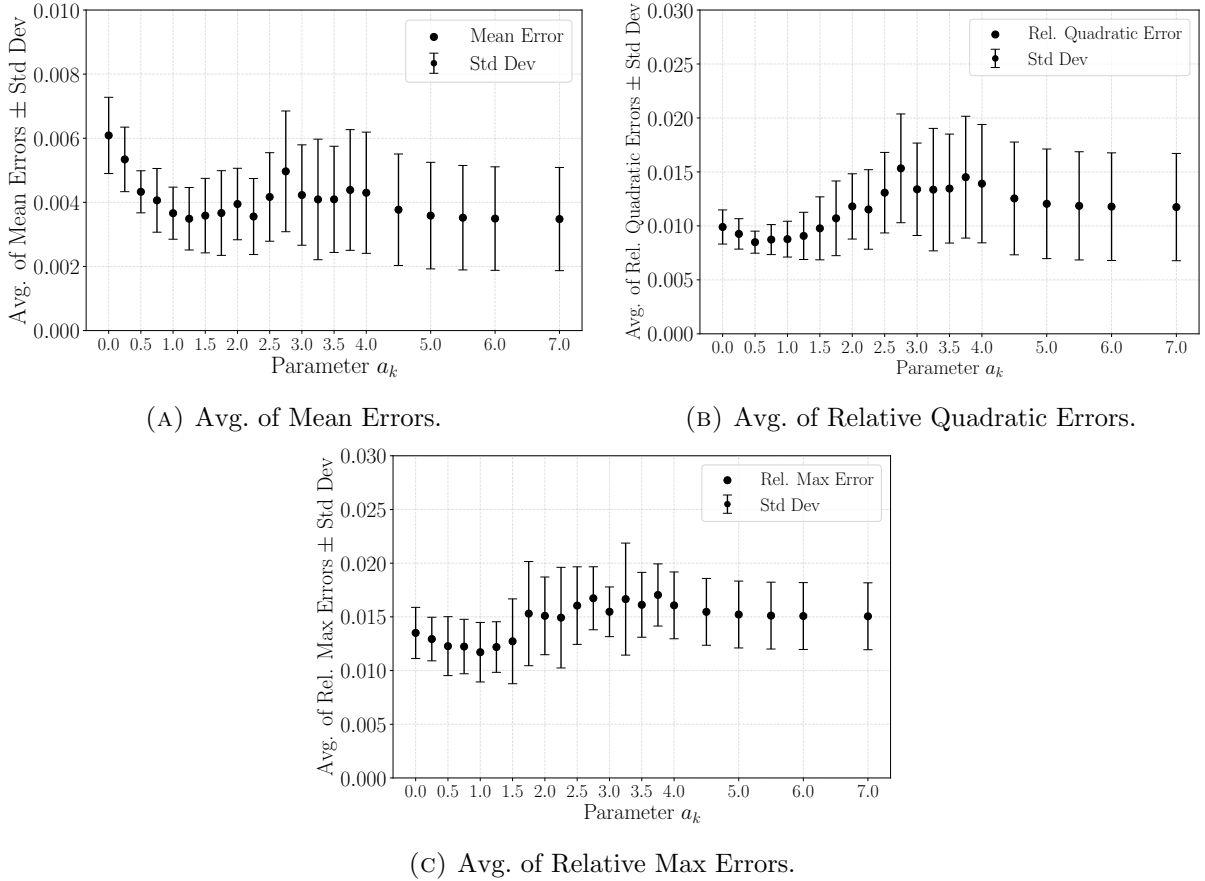


FIGURE 10. Average over ten network realisations  $\tilde{\Phi}_{\text{pred}}^{\text{pc}}$  of the prediction errors with respect to the polyconvex envelopes computed with the algorithm  $\tilde{\Phi}_\delta^{\text{pc}}$  for different values  $\alpha_k$  for the Saint Venant–Kirchhoff-based function  $\tilde{\Phi}$ .

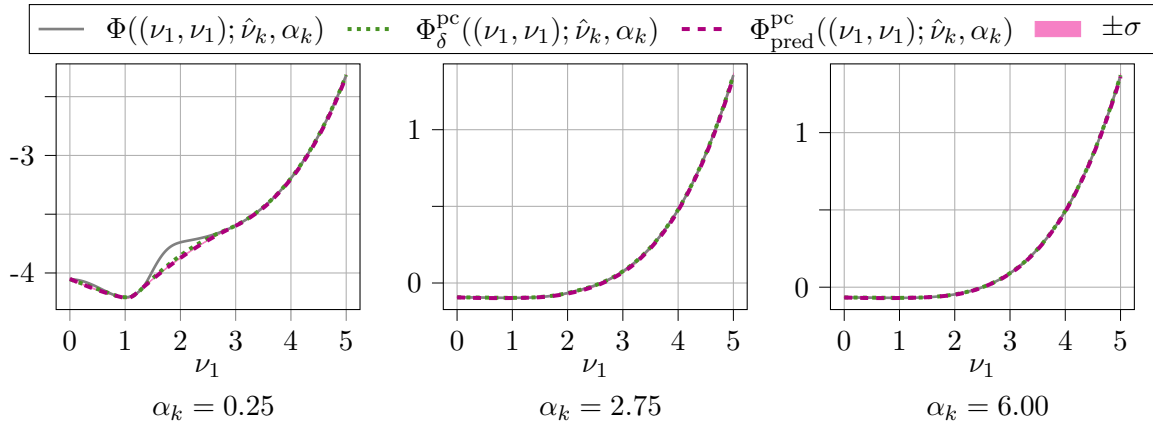


FIGURE 11. Comparison of the polyconvex envelopes  $\Phi_{\text{pred}}^{\text{pc}}$  (averaged over ten network realisations) and  $\Phi_{\delta}^{\text{pc}}$  for the Saint Venant–Kirchhoff model with  $\hat{\nu}_k = [2.5, 2.5]$  and for  $\alpha_k \in \{0.25, 2.75, 6.00\}$ . Plotted is the cross-section along the diagonal axis. The standard deviation of the ten predictions is marked by  $\sigma$ .

Once again, this number of parameters remains smaller than the storage required for only three polyconvex envelopes on a  $100 \times 100$  grid.

**6.5. Numerical Results for the Two-Dimensional Neo-Hookean Model.** We consider the function  $\Phi$  from (19) in the neo-Hookean based formulation, i.e.  $\psi^0$  from (3) is chosen and the material parameters are set as before. We aim for the representation of the function  $\tilde{\Phi}^{\text{pc}}: \mathbb{R}^d \times \mathbb{R}_+ \rightarrow \mathbb{R}$ , i.e. the polyconvex envelope of the normalised version (21), by a neural network.

**6.5.1. Network Architecture and Learning Data.** In this example, we implement a PICNN where each path consists of three hidden layers with 30, 60 and 60 neurons, respectively. The convex input, denoted by  $\hat{m}$ , represents the minors of the signed singular values  $\hat{\nu}_{k+1}$ , i.e.  $m(\hat{\nu}_{k+1})$ , while the nonconvex input, denoted as  $\zeta$ , corresponds to the parameter  $\alpha_k$ . The learning domain for  $\hat{\nu}_{k+1}$  is defined as  $[\nu_{\min}, \nu_{\max}]^2$  with  $\nu_{\min} = 0.01$  and  $\nu_{\max} = 18$ , while the learning domain for the parameter  $\alpha_k$  is  $[0, \alpha_{\infty}]$ . For the learning dataset, the set of points in the signed singular value space is obtained by discretising each axis as follows  $[\nu_{\min} : 0.01 : 2] \cup [2 : 0.05 : \nu_{\max}]$ , so that the grid is refined around the minimum, leading to a  $518 \times 518$  grid, and we choose the set of learning values  $\alpha_k$  as  $\mathcal{I}_{\alpha_k} = \{0, 0.1, \dots, 1.5, 1.7, 2, 2.5, 3, 3.5, 4\}$ , i.e. 22 values. These discretisations lead a learning dataset of 5,903,128 points. From this dataset, 70% of the samples are randomly assigned to the training set, while the remaining 30% constitute the validation set. The target values  $\Phi_{\delta}^{\text{pc}}$  are computed with the SVPC LP algorithm. The computation of the target values takes 4700 CPU hours. Figure 12 illustrates the target values along the axis  $(\nu_1, \nu_1)$ . For the loss function, we choose the penalty parameters  $\lambda_{\text{ineq}} = 1$  and  $\lambda_{\text{sym}} = 1$ .

**6.5.2. Numerical Results.** On average, for a single realisation, the training process requires 2.14 h  $\pm$  28 minutes to complete  $44 \pm 10$  epochs. The final training error is  $6.83 \times 10^{-5} \pm 2.38 \times 10^{-5}$ , while the validation error reaches  $7.30 \times 10^{-5} \pm 3.74 \times 10^{-5}$ . The learning curves for one of these realisations are presented in Figure 12.

Figure 13 illustrates the relative errors between the predictions and the polyconvex envelopes computed by the SVPC LP algorithm for different values of  $\alpha_k$ , including values that are outside the training domain. These errors are computed on a uniform  $100 \times 100$  discretisation of the domain  $[\nu_{\min}, \nu_{\max}]^2$ . Across all considered parameter sets, the errors remain consistently low, ranging between 1% and 2%. In particular, it is important to note that the hypothesis stating that the energies become independent of  $\alpha_k$  for  $\alpha_k \geq \alpha_{\infty}$  is verified and validates our choice of  $\alpha_{\infty} = 4$ . Additionally, Figure 14 provides an example of re-shifted predictions, i.e. application of (22). It has to be noted that the predictions are in good agreement with the polyconvex envelopes

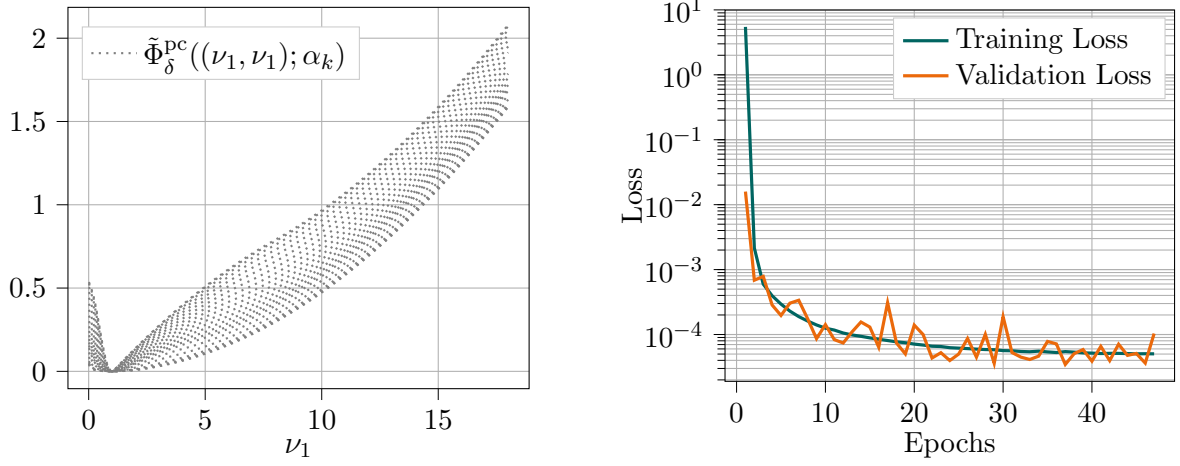


FIGURE 12. Left: Learning data for NH based damage. Diagonal cross-sections of the target values, i.e. polyconvex envelopes  $\tilde{\Phi}_\delta^{\text{PC}}$  for the neo-Hookean-based function  $\tilde{\Phi}$  with  $\alpha_k \in \mathcal{I}_{\alpha_k}$ . Right: Learning curves for NH-based damage. Learning curves based on  $\mathcal{L}$  from (15) for a single network initialisation for the neo-Hookean-based function  $\tilde{\Phi}_\delta^{\text{PC}}$ .

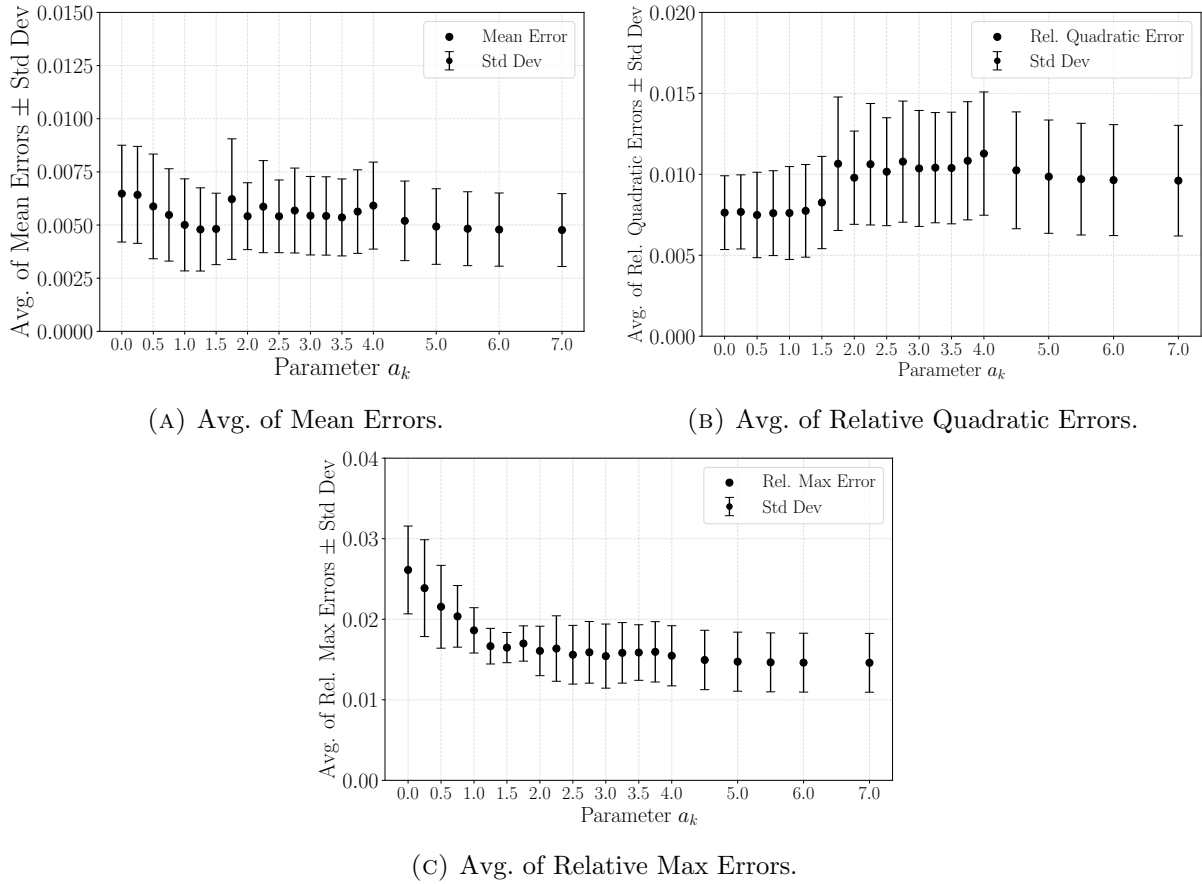


FIGURE 13. Average over ten network realisations  $\tilde{\Phi}_{\text{pred}}^{\text{PC}}$  of the prediction errors with respect to the polyconvex envelopes computed with the algorithm  $\tilde{\Phi}_\delta^{\text{PC}}$  for different values  $\alpha_k$  for the neo-Hookean-based function  $\tilde{\Phi}$ .

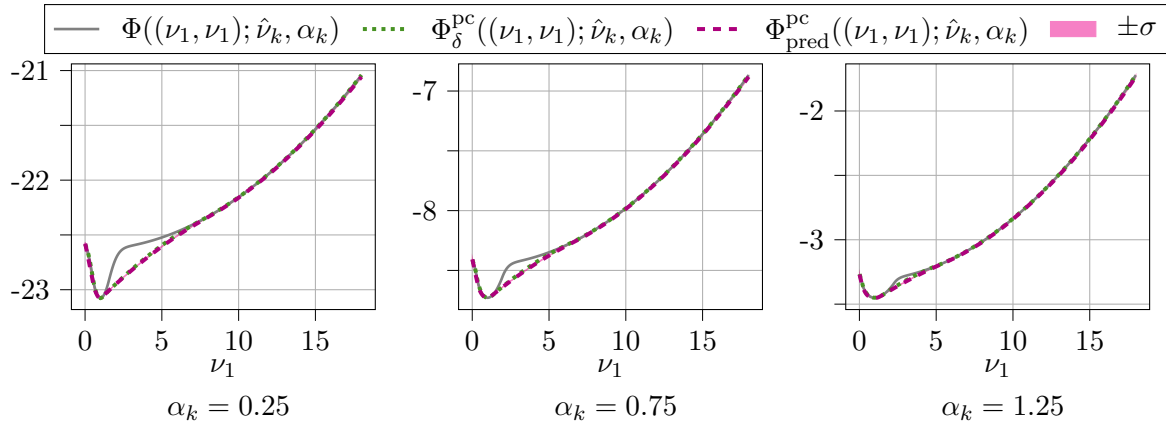


FIGURE 14. Comparison of the polyconvex envelopes  $\Phi_{\text{pred}}^{\text{pc}}$  (averaged over ten network realisations) and  $\Phi_{\delta}^{\text{pc}}$  for the neo-Hookean model with  $\hat{\nu}_k = [9, 9]$  and for  $\alpha_k \in \{0.25, 0.75, 1.25\}$ . Plotted is the cross-section along the diagonal axis. The standard deviation of the ten predictions is marked by  $\sigma$ .

computed by the SVPC LP algorithm from Section 6.3. For comparison, the computation of one polyconvex envelope on a  $100 \times 100$  grid using the SVPC LP algorithm takes 8.1 hours on one CPU while its prediction via neural networks takes only 0.2 seconds. As previously, the neural network implemented in this example contains 26,121 parameters, comprising both weights and biases. Once again, this number of parameters remains smaller than the storage required for only three polyconvex envelopes on a  $100 \times 100$  grid. These aspects once again emphasise the benefits of using a neural network based representation of the polyconvex envelope for parameter dependent families of functions for applications in engineering problems.

## 7. CONCLUSION

We have demonstrated the effectiveness of a neural network design in predicting polyconvex envelopes with high accuracy and computational efficiency. Our results show that such neural networks can generalise well beyond the learning dataset, enabling fast, multi-query evaluations and real-time computations. Moreover, we have introduced a splitting strategy which decouples the isotropic damage problem from the previous time step state, thereby improving the feasibility and robustness of the training process. Future research will focus on extending this framework to predict not only the polyconvex envelopes but also their derivatives as well as the incorporation of determinant constraints into the neural networks, as relevant for engineering applications in computational mechanics. The results presented in this paper pave the way for complex material simulations in real engineering contexts.

## ACKNOWLEDGEMENT

Many of the ideas in this paper were initially formulated and tested during Helena Althoff's Master's thesis [Alt24], and her contributions have been important in their refinement. Fruitful discussions with Daniel Balzani and Maximilian Köhler are gratefully acknowledged, and some ideas are the result of joint discussions with David Wiedemann.

## REFERENCES

- [AAF22] F. As'ad, P. Avery, and C. Farhat. A mechanics-informed artificial neural network approach in data-driven constitutive modeling. *International Journal for Numerical Methods in Engineering*, 123(12):2738–2759, 2022.
- [AF98] G. Allaire and G. Francfort. Existence of minimizers for non-quasiconvex functionals arising in optimal design. *Annales de l'Institut Henri Poincaré C. Analyse Non Linéaire*, 15(3):301–339, 1998.
- [AF23] F. As'ad and C. Farhat. A mechanics-informed deep learning framework for data-driven nonlinear viscoelasticity. *Computer Methods in Applied Mechanics and Engineering*, 417:Paper No. 116463, 19, 2023.

- [Alt24] Helena C. Althoff. Neuronale Netze für Konvexifizierung und Relaxierung von inkrementellen Spannungspotentialen. M.Sc. Thesis, University of Augsburg, Augsburg, Germany, 2024.
- [AXK17] B. Amos, L. Xu, and J. Z. Kolter. Input convex neural networks. In Doina Precup and Yee Whye Teh, editors, *Proceedings of the 34th International Conference on Machine Learning*, volume 70 of *Proceedings of Machine Learning Research*, pages 146–155. PMLR, 08 2017.
- [Bal76] John M. Ball. Convexity conditions and existence theorems in nonlinear elasticity. *Archive for Rational Mechanics and Analysis*, 63:337–403, 1976.
- [Bal77] John M. Ball. Constitutive inequalities and existence theorems in nonlinear elasto-statics. In R.J. Knops, editor, *Nonlinear Analysis and Mechanics: Heriot-Watt Symposium, Vol. 1*, volume 17 of *Pitman Research Notes in Mathematics Series*, pages 187–241. Pitman Books, London, 1977.
- [Bal02] J. M. Ball. *Some Open Problems in Elasticity*, pages 3–59. Springer New York, New York, 2002.
- [Bar04] S. Bartels. Linear convergence in the approximation of rank-one convex envelopes. *M2AN. Mathematical Modelling and Numerical Analysis*, 38(5):811–820, 2004.
- [Bar05] S. Bartels. Reliable and efficient approximation of polyconvex envelopes. *SIAM Journal on Numerical Analysis*, 43(1):363–385, 2005.
- [BEG15] T. Bosse, L. Eneya, and A. Griewank. An algorithm for pointwise evaluation of polyconvex envelopes II: generalization and numerical results. *Afrika Matematika*, 26(1-2):31–52, 2015.
- [BKN<sup>+</sup>24] D. Balzani, M. Köhler, T. Neumeier, M. A. Peter, and D. Peterseim. Multidimensional rank-one convexification of incremental damage models at finite strains. *Computational Mechanics*, 73(1):27–47, 2024.
- [BO12] D. Balzani and M. Ortiz. Relaxed incremental variational formulation for damage at large strains with application to fiber-reinforced materials and materials with truss-like microstructures. *International Journal for Numerical Methods in Engineering*, 92(6):551–570, 2012.
- [Cal20] O. Calin. *Deep learning architectures—a mathematical approach*. Springer Series in the Data Sciences. Springer, Cham, 2020.
- [CD18] Sergio Conti and Georg Dolzmann. An adaptive relaxation algorithm for multiscale problems and application to nematic elastomers. *Journal of the Mechanics and Physics of Solids*, 113:126–143, 2018.
- [CG22] P. Chen and J. Guilleminot. Polyconvex neural networks for hyperelastic constitutive models: A rectification approach. *Mechanics Research Communications*, 125:103993, 2022.
- [CSZ19] Y. Chen, Y. Shi, and B. Zhang. Optimal control via neural networks: A convex approach. In *International Conference on Learning Representations*, 2019.
- [Dol99] G. Dolzmann. Numerical computation of rank-one convex envelopes. *SIAM Journal on Numerical Analysis*, 36(5):1621–1635, 1999.
- [DW00] G. Dolzmann and N. J. Walkington. Estimates for numerical approximations of rank one convex envelopes. *Numerische Mathematik*, 85(4):647–663, 2000.
- [EBG13] L. Eneya, T. Bosse, and A. Griewank. A method for pointwise evaluation of polyconvex envelopes. *Afrika Matematika*, 24(1):1–24, 2013.
- [FJB<sup>+</sup>21] M. Fernández, M. Jamshidian, T. Böhlke, K. Kersting, and O. Weeger. Anisotropic hyperelastic constitutive models for finite deformations combining material theory and data-driven approaches with application to cubic lattice metamaterials. *Computational Mechanics*, 67(2):653–677, 2021.
- [GKWM25] G.-L. Geuken, P. Kurzeja, D. Wiedemann, and J. Mosler. Input convex neural networks: universal approximation theorem and implementation for isotropic polyconvex hyperelastic energies, 2025.
- [HCTC21] C-W Huang, R. T. Q. Chen, C. Tsirigotis, and A. Courville. Convex potential flows: Universal probability distributions with optimal transport and convex optimization, 2021.
- [KFM<sup>+</sup>22] D. K. Klein, M. Fernández, R. J. Martin, P. Neff, and O. Weeger. Polyconvex anisotropic hyperelasticity with neural networks. *Journal of the Mechanics and Physics of Solids*, 159:Paper No. 104703, 25, 2022.
- [KNM<sup>+</sup>22] M. Köhler, T. Neumeier, J. Melchior, M. A. Peter, D. Peterseim, and D. Balzani. Adaptive convexification of microsphere-based incremental damage for stress and strain softening at finite strains. *Acta Mechanica*, 233(11):4347–4364, 2022.
- [KNP<sup>+</sup>24] M. Köhler, T. Neumeier, M. A. Peter, D. Peterseim, and D. Balzani. Hierarchical rank-one sequence convexification for the relaxation of variational problems with microstructures. *Computer Methods in Applied Mechanics and Engineering*, 432:Paper No. 117321, 20, 2024.
- [KOMFW22] D. K. Klein, R. Ortigosa, J. Martínez-Frutos, and O. Weeger. Finite electro-elasticity with physics-augmented neural networks. *Computer Methods in Applied Mechanics and Engineering*, 400:Paper No. 115501, 33, 2022.
- [KS86a] R. V. Kohn and G. Strang. Optimal design and relaxation of variational problems. I. *Communications on Pure and Applied Mathematics*, 39(1):113–137, 1986.
- [KS86b] R. V. Kohn and G. Strang. Optimal design and relaxation of variational problems. II. *Communications on Pure and Applied Mathematics*, 39(2):139–182, 1986.

- [LK23] K. Linka and E. Kuhl. A new family of constitutive artificial neural networks towards automated model discovery. *Computer Methods in Applied Mechanics and Engineering*, 403:Paper No. 115731, 27, 2023.
- [LKK<sup>+</sup>23] L. Linden, D. K. Klein, K. A. Kalina, J. Brummund, O. Weeger, and M. Kästner. Neural networks meet hyperelasticity: A guide to enforcing physics. *Journal of the Mechanics and Physics of Solids*, 179:105363, 2023.
- [Mie95] C. Miehe. Discontinuous and continuous damage evolution in Ogden-type large-strain elastic materials. *European Journal of Mechanics. A. Solids*, 14(5):697–720, 1995.
- [NPPW24] T. Neumeier, M. A. Peter, D. Peterseim, and D. Wiedemann. Computational polyconvexification of isotropic functions. *Multiscale Modeling & Simulation*, 22(4):1402–1420, 2024.
- [TCT22] V. Tac, F. S. Costabal, and A. B. Tepole. Data-driven tissue mechanics with polyconvex neural ordinary differential equations. *Computer Methods in Applied Mechanics and Engineering*, 398:Paper No. 115248, 18, 2022.
- [TSRT22] V. Tac, V. D. Sree, M. K. Rausch, and A. B. Tepole. Data-driven modeling of the mechanical behavior of anisotropic soft biological tissue. *Engineering with Computers*, 38(5):4167–4182, October 2022.
- [VRPB25] H. Vijayakumaran, J. B. Russ, G. H. Paulino, and M. A. Bessa. Consistent machine learning for topology optimization with microstructure-dependent neural network material models. *Journal of the Mechanics and Physics of Solids*, 196:106015, 2025.
- [WP23] D. Wiedemann and M. A. Peter. Characterization of polyconvex isotropic functions. Preprint, arXiv:2304.08385 [math.AP] (2023), 2023.
- [WWS23] M. E. Wilhelm, C. Wang, and M. D. Stuber. Convex and concave envelopes of artificial neural network activation functions for deterministic global optimization. *Journal of Global Optimization*, 85(3):569–594, 2023.
- [Zha02] K. Zhang. An elementary derivation of the generalized Kohn-Strang relaxation formulae. *Journal of Convex Analysis*, 9(1):269–285, 2002.